**TITLE:** Dlg5 and Cadherins are key to peripheral glia integrity

**AUTHORS:** Das, Mriga, Cheng, Duo, Matzat, Till, and Auld, Vanessa J.

University of British Columbia, Vancouver, Canada

**CORRESPONDING AUTHOR:** Vanessa Auld auld@zoology.ubc.ca

**AUTHOR AFFILIATIONS:**

**Mriga Das**

Department of Zoology, University of British Columbia, Vancouver, Canada

mrigadas@zoology.ubc.ca

**Duo Cheng**

Department of Zoology, University of British Columbia, Vancouver, Canada

d.cheng@zoology.ubc.ca

**Till Matzat**

Department of Zoology, University of British Columbia, Vancouver, Canada

tillmat@gmx.de

**Vanessa J Auld**

Department of Zoology, University of British Columbia, Vancouver, Canada

auld@zoology.ubc.ca

**RUNNING TITLE (36/40 characters):** Dlg5 and Cadherins regulate peripheral glia, septate junction and barrier formation.

**AUTHOR CONTRIBUTIONS:** M.D., D.C. and V.J.A. designed research; M.D., D.C., T.M performed research; T.M provided TEM data; M.D., D.C. and V.J.A. analyzed data; M.D, D.C. and V.J.A. wrote the paper and contributed to manuscript editing.

**ACKNOWLEDGMENTS**

This work was supported by UBC Bioimaging facility (RRID: SCR_021304). Stocks were obtained from the Bloomington Drosophila Stock Center (NIH P40OD018537) and the Vienna Drosophila Resource Center (VDRC, **www.vdrc.at**). This research was funded by a grant from the Natural Sciences and Engineering Research Council of Canada (NSERC) and the Canadian Institutes of Health Research (CIHR).

**CONFLICT OF INTEREST STATEMENT:** No competing interests

**KEY WORDS:** glia, adherens junctions, peripheral nerve,

Number of figures: 10

Number of tables: 1

**ABSTRACT**

Glial cells in the peripheral nerve wrap axons to insulate them and ensure efficient conduction of neuronal signals. In the myelin sheath, it is proposed that the autotypic tight junctions and adherens junctions form glia-glia complexes that stabilize the glia sheath in myelinating glia. Yet the role of adhesion junctions in non-myelinating glia of vertebrates or invertebrates has not been clearly established. Many components of adhering junctions contain PDZ (PSD-95, Dlg, ZO1) domains or are recruited to these junctions by PDZ binding motifs. To test for the role of PDZ domain proteins in glial sheath formation, we carried out an RNAi screen using *Drosophila melanogaster* to knockdown each of the 66 predicted PDZ domain proteins in the peripheral glia. We identified six PDZ genes with potential roles in glial morphology, and further investigated Discs-large 5 (Dlg5), a scaffolding protein with no previously known function in glia. Knockdown of Dlg5 disrupts subperineurial glia (SPG) morphology, including gaps in the membrane that coincide with disruption of septate junction proteins. To further our investigation of Dlg5, we focused on cadherins and found both N-Cadherin and E-Cadherin are expressed throughout peripheral glia. Knockdown of E-Cadherin phenocopied the loss of Dlg5 leading to gaps in the SPG and septate junctions while only simultaneous loss of both N-Cadherins (NCad, and CadN2) had the same effect. The loss of all three Cadherins enhanced these phenotypes as did loss of Dlg5 when paired with cadherin knockdown. This leads to a model where Dlg5 plays a role in conjunction with cadherins in glial membrane stabilization and septate junction formation in the subperineurial glia.

**INTRODUCTION:**

A critical function of glia is to wrap and ensheath axons in both the central and peripheral

66 nervous systems. In vertebrate peripheral nerves, myelinating Schwann cells enable rapid and
67 efficient transduction of electrical signals by forming the myelin sheath to ensheath and insulate
68 large caliber axons. While there are extensive studies that have identified the protein complexes
69 that mediate myelin sheath formation and stabilization, almost nothing is known about the
70 adherent junctions that mediate sheath formation in non-myelinating Schwann cells. Yet this
71 class of glia is essential to protect and support small calibre axons such as C-fibers that transmit
72 nociceptive information (Chen et al., 2003; Griffin and Thompson, 2008).

73 Many components of adherent junctions such as tight junctions (TJ) are either PDZ (PSD-95,
74 Dlg, ZO1) proteins or contain motifs allowing for interactions with PDZ proteins. PDZ domains
75 are 80-90 amino acids and mediate protein-protein interaction by binding to short three amino
76 acid PDZ binding motifs found at the C-terminus of many proteins (Harris and Lim, 2001;
77 Subbaiah et al., 2011). Many PDZ proteins possess different combinations of protein interaction
78 domains that mediate the recruitment of protein complexes. For instance, the family of
79 membrane-associated guanylate kinases (MAGUKs) apart from PDZ domains, possess L27, SH3
80 and GUK domains. PDZ proteins regulate processes such as cell polarity, adhesion, migration
81 and signalling through their ability to scaffold proteins in specific regions of the cell. It is likely
82 that PDZ proteins play a role in mediating non-myelinating glia junctions and are critical for
83 glial cell function.

84 Acquiring a better understanding of PDZ proteins and their role in glial junctions requires
85 that we identify those PDZ proteins that function in non-myelinating glia. Our model is the
86 peripheral nerve of *Drosophila melanogaster* given that there are only 66 PDZ proteins in
87 Drosophila (Aranjuez et al., 2012 2001) (compared to the 250 predicted PDZ proteins in humans
88 (Tonikian et al., 2008)) and that *Drosophila* peripheral glia are an excellent model to further our

89 understanding of the mechanisms underlying non-myelinating glia development and function.
90 Each peripheral nerve is ensheathed by three glial layers. The innermost glia layer, the wrapping
91 glia (WG) resemble non-myelinating Schwann cells and extend their processes around individual
92 or bundles of motor and sensory axons. The wrapping glia layer is surrounded by the
93 subperineurial glia (SPG), which form septate junctions between the glial layers to establish the
94 blood-nerve barrier to protect peripheral axons from the high K+ hemolymph (Auld et al., 1995;
95 Baumgartner et al., 1996). Septate junctions form a ladder-like array of a core protein complex
96 that is conserved with paranodal junctions including Neurexin IV, Neuroglian and Contactin
97 (Bhat, 2003; Limmer et al., 2014). Lastly, the perineurial glia (PG), which are the equivalent to
98 vertebrate perineurial cells, wrap the nerve and adhere to the extracellular matrix that surrounds
99 and stabilizes the entire nerve. Adhesion and signalling between these different glial layers must
100 require glia-glia interactions, however the proteins and in particular the PDZ proteins required
101 for these processes in remain largely unknown.
102 In this study, we screened all 66 Drosophila PDZ-encoding proteins using RNAi knockdown
103 to determine which play a role in peripheral glia. We identified seven PDZ domain proteins
104 where loss of function lead to disruption of peripheral glia and focused our subsequent
105 investigation on Discs-large 5 (Dlg5). Dlg5 is a MAGUK protein with a coiled-coil domain at
106 the amino terminus, four PDZ domains, an SH3 and GUK domain, and has been implicated in
107 cell polarity and Cadherin complex formation (Nechiporuk et al., 2007; Wang et al., 2014; Reilly
108 et al., 2015; Liu et al., 2017). The role of Dlg5 and those of the classical Cadherins in non-
109 myelinating glia, including the peripheral glia of Drosophila, had not been determined.
110 Therefore, we went onto investigate Dlg5 and potential functional overlap with the Drosophila
111 classical cadherins; E-Cadherin (ECad, *shotgun*), N-Cadherin (NCad, *CadN*), N-Cadherin2

112 (NCad2, *CadN2*) in the three layers of peripheral glia. Knockdown of Dlg5 in the subperineurial
113 glia resulted in breaks/gaps within the glial membrane and disruption of septate junction
114 proteins. We found that ECad, NCad and CadN2 perform redundant functions in the
115 subperineurial glia, and that loss of Cadherins phenocopied and enhanced the loss of Dlg5
116 phenotypes. Overall, our results show that Dlg5 interacts with cadherins to mediate SPG and
117 septate junction morphology.
118

119 **MATERIALS AND METHODS:**

120 **Fly strains and genetics**

121 The following fly strains were used in this study: repo-GAL4 (Sepp et al., 2001); Nrv2-GAL4
122 (Sun et al., 1999), 46F-GAL4 (Xie and Auld, 2011); Gli-GAL4 (Sepp and Auld, 1999); SPG-
123 GAL4 (Schwabe et al., 2005); UAS-mCD8::GFP (Lee and Luo, 1999); UAS-Dicer2 (Dietzl et
124 al., 2007); *Df(2L)BSC148*, UAS-mCD8::RFP, UAS-Dlg5::GFP (Bloomington Stock Center,
125 BDSC). The following GFP and RFP protein-trap insertions were used: Dlg5::GFP (Sarov et al.,
126 2016); Nrv2::GFP, NrxIV::GFP, Scrib::GFP (Morin et al., 2001; Kelso et al., 2004; Buszczak et
127 al., 2007); NCad::cherry, ECad::cherry (Venken et al., 2011). The following RNAi lines were
128 used and those lines preferentially used for the majority of experiments are in bold: Dlg5-RNAi
129 (VDRC: **46234**, 101596; BDSC: 41832); Arm-RNAi (VDRC: 7767, **107344**); ECad-RNAi
130 (VDRC: **27802**; 103962; BDSC: 27689, 32904, 38207); NCad-RNAi (VDRC: **1092**; BDSC:
131 27503); CadN2-RNAi (VDRC: 101659; BDSC: **27508**); Crumbs-RNAi (VDRC: **39177**). All
132 RNAi experiments carried out after the initial screen were raised at 25°C either with or without

133 Dicer2 in the background. For all experiments, controls were the driver line crossed with
134 *w[1118].*
135
136 **Screen of RNAi knockdown of PDZ genes:** RNAi lines were obtained from TRiP and VDRC
137 stock centers. Table 1 provides the list of RNAi lines used in the screen.
138 *repo>mCD8::RFP/TM6,Tb* virgin flies were crossed with males from each UAS-RNAi line at
139 29°C. As a control, *repo>mCD8::RFP/TM6,Tb* virgin flies were crossed with $w^{1118}$ males and
140 raised at 29°C. A minimum of 6 larvae were dissected from each cross and stained with mAb
141 22C10 (anti-Futsch) to label the peripheral axons. The morphology of the glial membranes were
142 visualized using UAS-mCD8::RFP.
143
144 **Immunolabeling and image analysis:** The peripheral nervous system of 3rd instar, wandering
145 larvae were dissected and fixed for immunolabeling using previously described methods (Sepp et
146 al., 2000). The following primary antibodies were used in this study: guinea pig anti-Inx2
147 (1:500) (Smendziuk et al., 2015); mouse anti-Futsch/22C10 (1:1000, DSHB); rabbit anti-GFP
148 (1:600, Life Technology); mouse anti-GFP (1:300, Novus Biologicals), rabbit anti-Cherry
149 (1:300, Abcam), mouse anti-βPS (1:50, CF.6G11) (Brower, 1984), rabbit anti-HRP (1:500,
150 Jackson ImmunoResearch, West Grove, PA); mouse anti-Futsch/22C10 (1:1000, DSHB); rabbit
151 anti-Nrv2.1 (1:1000, Abcam). The following secondary antibodies were used at a 1:300 dilution:
152 goat anti-mouse Alexa 488, Alexa 568 and Alexa 647; goat anti- rabbit Alexa 568 and goat anti-
153 guinea pig Alexa 647 (Molecular Probes). DAPI (1:1000, Invitrogen) was used to label nuclei.
154 Images were acquired with a Delta Vision Spectris compound microscope (Applied
155 Precision/GE Healthcare, Mississauga, Ontario) using a 60x oil immersion objective (NA 1.4).

156 An image was captured every 0.2 µm and the resulting stacks were deconvolved (SoftWorx,
157 Toronto, Canada) using a point spread function measured with 0.2 µm beads conjugated to Alexa
158 dyes (Molecular Probes) and mounted in Vectashield (Vector Laboratories, Burlington, Canada).
159 Cross sections were generated using SoftWorx. A single z-slice was chosen from each z-stack
160 and images were compiled using Adobe Photoshop and Adobe Illustrator CC. For transmission
161 electron microscopy analysis larvae were dissected and prepared using previously described
162 methods (Matzat et al., 2015) using a Hitachi H7600 TEM at the UBC BioImaging Facility.
163
164 **Dye Penetration Assay:** Third instar larvae were washed using 1X PBS, then opened at the
165 posterior end and inverted in Schneider's insect medium (Millipore Sigma, S0146). The inverted
166 larvae were incubated in Schneider's medium containing 2.5 mM of 10,000MW Dextran Texas
167 Red-conjugated dye (Invitrogen, D1863, Lysine Fixable) for 40 minutes at room temperature on
168 an orbital shaker. The larvae were then fixed using 4% PFA with 1X PBS for 20 minutes.
169 Following fixation, samples were washed with 1X PBS twice for 5 minutes each, then washed
170 with 0.1% PBST with 1X PBS twice for 10 minutes each. Lastly, the brains were dissected and
171 mounted in Vectashield. The samples were imaged using an Olympus FV1000 Confocal
172 microscope (BioImaging Facility UBC) using a 30X Silicone oil immersion objective (NA =
173 1.05) with 1um steps. Laser (559nm) intensity was set at 7% intensity, 750V digital gain, 1x
174 master Gain, and 6% offset for all genotypes except for imaging of NrxIV-RNAi, which was 5%
175 intensity, 750V digital gain, 1x master Gain, and 6% offset. Images were imported into ImageJ
176 and fluorescence intensity calculated and images displayed using the Fire Look up Table.
177

178 **Locomotion assay:** Locomotion assays were performed using third instar larvae adapted from
179 (Brooks et al., 2016). Larvae of the desired genotype were gently placed onto a freshly made 2%
180 agar plate with food-safe dye added to enhance contrast. Larval movements were recorded
181 continuously for 60 seconds using a Canon VIXIA HF R800 video camera. The recordings were
182 then converted from *.MOV to *.AVI files using FFmpeg (ffmpeg.org) and analyzed using the
183 wrMTrck plug-in (Nussbaum-Krammer et al., 2015; Brooks et al., 2016) in Fiji to calculate
184 locomotion and movement trajectory. Larvae with non-continuous paths throughout the entirety
185 of the recording were discarded from the total travel distance quantification but were included in
186 the average travel speed.
187
188 **Statistics:** Prism (GraphPad Software) was used for all statistical analyses and a One-way Anova
189 utilized to compared multiple genotypes with the specified control with a Dunnet multiple
190 comparison test. For comparisons across multiple genotypes a Tukey multiple comparison test
191 was used. For TEM data analysis a Kruskal-Wallis non-parametric test with a Dunn's multiple
192 comparisons test was utilized. For all fluorescence image analyses at least 6-7 nerves were
193 analyzed per larvae.
194
195 **RESULTS**
196 ***RNAi induced knockdown of PDZ proteins in glial cells***
197 To understand the role of PDZ proteins in mediating glia interactions, we utilized the peripheral
198 nerve of the 3rd instar *Drosophila* larva to investigate the consequences on glial morphology of
199 knockdown of PDZ domain proteins. There are 66 genes predicted to encode PDZ domain
200 proteins in the *Drosophila* genome (Aranjuez et al., 2012). Using the pan-glial driver *repo-*

201 *GAL4*, we expressed each *UAS-PDZ-RNAi* line while co-expressing *UAS-mCD8::RFP* to label
202 the glial membranes. We scored morphological defects in the labeled peripheral glial membranes
203 and axons were labeled using anti-Futsch to reveal any axonal defects. When available, multiple
204 RNAi lines were used to target each PDZ gene. For the 66 genes, 150 individual *UAS-RNAi* lines
205 were tested for abnormal glial phenotypes in the PNS (Fig.1A, Supplemental Table 1). As a
206 control *repo>mCD8::RFP* flies were crossed to $w^{1118}$ flies (Fig. 1B-B'). We classified PDZ
207 genes as positive hits (Fig. 1A; Supplemental Table 1) if their knockdown using multiple RNAi
208 lines resulted in lethality or glial phenotypes. Seven PDZ proteins; Discs Large 1 (Dlg1),
209 Scribbled (Scrib), Varicose (Vari), Stardust (sdt), Discs Large 5 homolog (Dlg5), Locomotion
210 defects (loco), and a Rho-type guanine nucleotide exchange factor (RhoGEF2) were identified as
211 positive hits with potential functions in glial cells (Fig. 1A,C-G; Supplemental Table 1). The
212 screen resulted in a range of phenotypes such as glial swelling observed with the knockdown of
213 RhoGEF2 and Loco (Fig. 1C-C", F-F"). Knockdown of Dlg1 and Scrib resulted in abnormal
214 axonal wrapping (Fig.1 D-D", E-E"), whereas Vari knockdown in all glia was lethal (Table 1).
215 Abnormalities in axonal wrapping, specifically by the inner wrapping glial membrane were
216 observed with Dlg5 knockdown (Fig. 1G-G'). Of note is that loss of known apical polarity
217 proteins including Bazooka (baz, Par-3), Par-6 and Patj had no effect (Fig. 1A; Supplemental
218 Table 1). Conversely the basolateral polarity proteins such as Dlg1 and Scrib had strong effects
219 as did Dlg5, which is also thought to function in epithelial polarity (Luo et al., 2016). Overall, we
220 identified a group of PDZ proteins that may play necessary roles in peripheral glia development
221 and a number of these proteins are known to function in polarity and junction formation.
222
223 ***Dlg5 is expressed in glial cells of the larval peripheral nerve***

224 Given the role of Dlg5 in cell polarity and cell-cell adhesion, and the fact that Dlg5 has not been
225 studied in glia, we chose to investigate Dlg5 further. Dlg5 is a MAGUK protein with a coiled-
226 coil domain at the amino terminus, four PDZ domains, an SH3 and GUK domains. We began by
227 examining the distribution of Dlg5 in the glial layers of the peripheral nerve in 3rd instar larvae
228 using Dlg5 endogenously tagged with GFP (Dlg5::GFP)(Sarov et al., 2016). Dlg5 puncta were
229 observed throughout the peripheral nerve, with puncta present within the glial cell membranes
230 (identified with mCD8::RFP) (Fig. 2A-A"). Some Dlg5 puncta might also be present in the
231 axons (immunolabeled with anti-futsch) (Fig. 2B-B"). However, knockdown of Dlg5 using the
232 pan-neuronal driver elav-GAL4, did not affect either peripheral glial or axon morphology (n=6
233 larvae).

234 To further characterize the effects of Dlg5 loss in the peripheral glia, we knocked down Dlg5
235 in individual glial layers using GAL4 drivers specific to each of the three glial layers driving a
236 membrane marker, mCD8::RFP. We tested multiple RNAi lines and used the strongest RNAi
237 line, 46234, for this and future experiments. Knockdown of Dlg5 in the PG using 46F-GAL4
238 (*46F>mCD8::RFP,Dlg5-RNAi*) (n=5 larvae) did not affect PG membrane morphology (Fig. 2D-
239 D") compared to control (*46F>mCD8::RFP*)(Fig 2A-A")(n=7 larvae). Knockdown of Dlg5
240 using Gli-GAL4 in the intermediate SPG layer (*Gli>mCD8::RFP,Dlg5-RNAi*) disrupted SPG
241 morphology (Fig. 2F,F"), but had no effect on the WG (marked with Nrv2::GFP) (Fig. 2F')(n=6
242 larvae). SPG membrane morphology was disrupted in 16.5% of nerves, with breaks/gaps in the
243 membrane (yellow arrows) and occasionally accompanied by swellings (Fig. 2F,F", asterisks).
244 The control (*Gli>mCD8::RFP*) did not have any defects (Fig. 2E-E")(n= 6 larvae). Knockdown
245 of Dlg5 in the WG using Nrv2-GAL4 (*Nrv2>mCD8::RFP,Dlg5-RNAi*) resulted in reduced and
246 discontinuous WG strands in 53% of nerves (Fig. 2H") (n=5 larvae) compared to the control

247 nerves (*Nrv2>mCD8::RFP*), where multiple, continuous WG strands ensheath the axons (Fig.
248 2G")( n=6 larvae). Dlg5 knockdown in the WG did not affect axonal morphology (Fig. 2H')
249 which was similar to control nerves (Fig. 2G'). Overall, our results suggest the Dlg5 is expressed
250 in multiple peripheral glia and is required in both the SPG and the WG but not in the PG layer.
251

252 ***Dlg5 is required for the formation of septate junctions***

253 Since Dlg5 knockdown affected SPG morphology, we next tested if the defects in the SPG
254 extended to the septate junction (SJ) protein complex, which in Drosophila forms the blood-
255 nerve and blood-brain barriers. Using a range of SJ proteins we looked for changes in the SJ
256 morphology while knocking down Dlg5 in the SPG (*Gli>mCD8::RFP, Dlg5-RNAi*). For
257 multiple RNAi lines (101596, 41832, 46234), we observed nerves with gaps in the SJ strands
258 when labeled with NrxIV::GFP (Fig. 3B-B") or immunolabeled with Nrv2.1 (Fig. 3D,D") and
259 often these corresponded to gaps in the mCD8::RFP labeled membrane (Fig. 3B",D") (n=12
260 larvae). In comparison, intact and continuous SJs were observed along the length of control
261 nerves (*Gli>mCD8::RFP* )(Fig. 3A-A",C-C") (n=12 larvae). Increasing the efficiency of the
262 RNAi with Dicer2 paired with a stronger SPG driver, moody-GAL4, increased the severity of the
263 phenotypes (*SPG>mCD8::RFP,Dlg5-RNAi,Dicer2*) and NrxIV::GFP was often observed in
264 large aggregates that corresponded to glial membrane concentrations (Fig. 3E-E"). We
265 quantified the percentage of nerves per larvae (using moody-GAL4) that had disrupted SPG or
266 gaps. On average 80% of the nerves were affected and with Dicer2, the penetrance was
267 increased to 100% (Fig. 3F). To determine if the effect to Dlg5 in the SPG was cell autonomous,
268 we knocked down Dlg5 in the PG and WG and assayed SJs using either *NrxIV::GFP* or the
269 Nrv2.1 antibody. The morphology of SJs was not affected by the knockdown of Dlg5 in the PG

270 layer (*46F>mCD8::RFP, Dlg5-RNAi*) (n=6 larvae). Similarly, knockdown of Dlg5 in the WG
271 (*NrxIV::GFP, Nrv2>mCD8::RFP, Dlg5-RNAi*) lead to the expected WG phenotypes, but did not
272 affect the morphology of the SJ strands (n= 6 larvae). Therefore, loss of Dlg5 in the SPG leads to
273 a range of defects in the SPG including disruption of the SJs in a cell autonomous manner.
274
275 ***Dlg5 associates with Drosophila N-Cadherin and E-Cadherin***
276 Prior studies have suggested that Dlg5 can interact in a number of cell types with β-catenin and
277 cadherin family members. Specifically Dlg5 is found co-localized with cadherins (Liu et al.,
278 2017), is involved in trafficking of cadherin-catenin adhesion complexes (Nechiporuk et al.,
279 2007; Wang et al., 2014; Reilly et al., 2015), and links the vinexin-vinculin complex and beta-
280 catenin at adherens junctions (Wakabayashi et al., 2003). We tested the possibility that Dlg5 also
281 interacts with cadherins in peripheral glia. The presence and distribution of cadherins in
282 Drosophila peripheral glia had not been established, so we began by looking for the presence of
283 the two classical Drosophila cadherins; E-Cadherin (ECad; *shotgun*) and N-Cadherin (NCad;
284 *CadN*) using genes endogenously tagged with mCherry or GFP (ECad::mCherry, ECad::GFP
285 and NCad::mCherry (Venken et al., 2011)). Both NCad and ECad puncta were observed
286 throughout the peripheral nerve (Fig. 4A,B) with both cadherins forming occasional short belt-
287 like patterns in some parts of the nerve. More frequently, NCad and ECad were observed in
288 puncta and we observed cadherin puncta throughout all glial layers (Fig. 4A-B, yellow arrows).
289 The majority of the NCad (Fig. 4C') and ECad (Fig. 4C") puncta were distinct with minimal co-
290 localization (Fig. 4C). The NCad and ECad puncta likely represent glial spot Adherens Junctions
291 (sAJ) (Matzat et al., 2015) and these were observed between the three different glial layers with
292 the majority occurring between the PG-SPG and SPG-WG processes (Fig. 4D, E)

293 Next, we tested for Dlg5 and cadherin co-localization using Dlg5::GFP crossed with
294 NCad::cherry (Fig. 4F) or ECad::cherry (Fig. 4G). Some but not all NCad (Fig. 4F'-F") and
295 ECad (Fig. 4G'-G") puncta overlapped with Dlg5 in the peripheral nerve (yellow arrows). This
296 partial overlap between NCad and Dlg5 is consistent with prior work in mouse embryonic
297 fibroblasts, where Dlg5 only overlapped with a subset of NCad (Wang et al., 2014). In
298 fibroblasts, Dlg5 is also partially associated with Rab11, a marker for recycling endosomes, as
299 they fuse with cadherin-containing vesicles. To test whether Dlg5 in Drosophila peripheral glia
300 are involved in trafficking pathways, we immunolabeled for a series of vesicle markers including
301 Rab11, Rabsn5 (an early endosomal marker), Rab7 (a late endosomal maker), HRS (a
302 multivesicular body (MVB) marker), Vps26 (a component of the retromer complex), Sec23 (a
303 COPII vesicle marker), G130 (a Golgi maker) as well as syntaxin1A (a t-SNARE protein) (Supp
304 Fig. 1). None of these subcellular markers consistently overlapped with Dlg5::GFP puncta in the
305 peripheral nerve (Supp Fig. 1).
306 Dlg5 has been found associated with SJ proteins such as Dlg1 and Neurexin-IV (Nrx-IV) in
307 Drosophila border cells (Liu et al., 2014a), yet in the peripheral glia Dlg5 did not localize with
308 these proteins at the SJ. Therefore, we wanted to test to see if Dlg5 was associated with any other
309 junctional complexes including gap junctions and focal adhesions (Supp Fig. 2). However, we
310 did not observe any co-localization between the Dlg5::GFP and gap junctions immunolabeled
311 with Inx2 (Supp Fig. 2C-C") nor with focal adhesions, immunolabeled for the integrin beta-
312 subunit βPS (Supp Fig 2D-D"). Therefore, Dlg5 is unlikely to be part of the gap junction or focal
313 adhesion complex. In addition, pan-glial knockdown of Dlg5 had no effect on Inx2 labeled gap
314 junctions, or βPS labeled focal adhesions. Overall, our results suggest that of the potential

315 junctional domains in peripheral glia, Dlg5 is the most frequently associated with cadherins.
316 However, this association appears to be limited to a subset of NCad and ECad.
317
318 ***E-Cadherin is required in glial cells of larval peripheral nerve***
319 To determine whether Dlg5 and cadherins work in a similar pathway, we next examined the
320 function of NCad and ECad in the peripheral nerve. To assay for abnormalities in glial
321 morphology, *repo-GAL4* was used to express RNAi and label the glial membranes with
322 mCD8::GFP and immunolabeling for Dlg1 used to assess SJ morphology. Normal glial
323 morphology and Dlg1 distribution was observed in all the control nerves (*repo>mCD8::GFP,*
324 *Dicer2*) (n=6 larvae) (Fig. 5A-A"). Pan-glial knockdown of ECad (*repo>ECad-RNAi, Dicer2*)
325 using multiple RNAi lines resulted in disrupted glial membranes and the appearance of "hole-
326 like" structures within the glial membrane in 71.4% nerves of the strongest RNAi (27082; n= 4
327 larvae) (Fig. 5B'). Dlg1 was mislocalized in 72% of the affected nerves (n=4 larvae) (Fig. 5B").
328 Surprisingly, knockdown of NCad (*repo>NCad-RNAi, Dicer2*) using multiple RNAi lines did
329 not affect glial morphology or Dlg1 distribution (data not shown).
330 To determine if ECad is required in one or all glial layers, we knocked down ECad in
331 individual glial layers using the strong ECad-RNAi line (27082). ECad knockdown in the
332 wrapping glia using Nrv2-GAL4 paired with Dicer2 resulted in fewer and discontinuous
333 wrapping glia strands in 89% of nerves (*Nrv2>ECad-RNAi, Dicer2*) (n=4 larvae) (Fig. 5D).
334 Axon morphology was not affected by the knockdown of ECad (Fig. 5D"). Control nerves
335 (*Nrv2>Dicer2*) had the expected multiple, continuous wrapping glia strands ensheathing the
336 peripheral axons (Fig. 5C). Therefore, ECad is required in the wrapping glia and is necessary for
337 axon ensheathment. Similar to the pan-glial knockdown of NCad, knockdown in the wrapping

338 glia did not affect glial morphology and the morphology of the axons was comparable to the
339 control. We next tested the function of ECad in the SPG layer using the SPG driver, Gli-GAL4,
340 to drive RNAi and label the SPG membranes with mCD8::RFP. The SPG membranes observed
341 in all control nerves (*Gli>mCD8::RFP, Dicer2*) were continuous and Dlg1 was correctly
342 localized to the septate junction (n= 6 larvae) (Fig. 5E). In comparison knockdown of ECad in
343 the SPG (*Gli>ECad-RNAi, Dicer2*) resulted in nerves with discontinuous SPG membranes (Fig.
344 5F) (n=6 larvae). The gaps in the SPG membrane coincided with the loss of Dlg1 (Fig. 5F',F";
345 yellow arrows). Therefore, ECad is required in the SPG for proper ensheathment and SJ
346 formation while the knockdown of NCad had no effect.
347 ECad knockdown affected SPG morphology and resulted in SPG defects similar to those
348 observed with the knockdown of Dlg5. To further characterize and quantify these phenotypes,
349 we used NrxIV::GFP as a marker to assess any changes in the SJ when E-Cad was knocked
350 down in the SPG (*moody>mCD8::RFP, ECad-RNAi*). Similar to the loss of Dlg5, ECad
351 knockdown results in gaps or breaks and aggregates of NrxIV::GFP within the SJ strands in 48%
352 of nerves (Fig. 6C-C') along with disruption to the glial membrane (Fig. 6C",D")(n=6 larvae).
353 Increasing the efficiency of the knockdown with Dicer2 (*moody>mCD8::RFP, ECad-RNAi,*
354 *Dicer2*) strengthened the phenotypes to the point where NrxIV::GFP was frequently observed in
355 aggregates (Fig. 6E-E',F-F'; yellow arrows) and the SPG membrane appeared collapsed (Fig.
356 6E",F"). The SJ strands in controls (*moody>mCD8::RFP, Dicer2*) were continuous and
357 NrxIV::GFP aggregates were never observed (Fig. 6A-A') (n=10 larvae). The presence of gaps
358 or disruption to the SJ was quantified and the percentage of nerves with SJ gaps was significantly
359 higher compared to controls (Fig. 6B).
360

361 ***N-Cadherins play redundant roles in the larval peripheral nerve***

362 Although NCad is expressed in the peripheral nerve, knockdown of NCad did not affect glial
363 morphology. There are two NCad loci in *Drosophila*, CadN (N-Cad) and a duplication CadN2
364 (N-Cad2) (Prakash et al., 2005). CadN2 shares 72.5% amino acid sequence identity and is
365 partially redundant to NCad (Yonekura et al., 2007). Therefore, it is possible that the loss of N-
366 Cad is compensated by CadN2. We knocked down CadN2 in all glia using multiple RNAi lines
367 (*repo>CadN2-RNAi*) and similar to N-Cad knockdown, CadN2 knockdown did not affect glial
368 morphology. To test for redundancy between these genes, we knocked down both NCad and
369 CadN2 in the SPG (*moody>NCad-RNAi, CadN2-RNAi*) and assayed for *NrxIV::GFP* labeled
370 SJs. We found that reducing the levels of both NCad and CadN2 resulted in defects in 35% of
371 the nerves (Fig. 7B-B'') (n=8 larvae). When we quantified the number of nerves that contained
372 gaps or breaks in the SJ, 13.5% of nerves were affected (Fig. 7E), which was significantly
373 greater than either RNAi alone or control.

374 These defects were similar to those we observed with the knockdown of ECad in the SPG
375 suggesting that NCad and CadN2 are not only redundant with each other but also perform some
376 of the same functions as ECad. To test if ECad and NCad are redundant, we performed a double
377 knockdown of NCad and ECad in the SPG (*moody>NCad-RNAi, ECad-RNAi)*. Knockdown of
378 NCad significantly enhanced the ECad-RNAi phenotypes compared to either RNAi line alone
379 (n=6 larvae) (Fig. 7E). To further test if all three cadherins perform similar functions in the
380 peripheral glia, we knocked down ECad in conjunction with a heterozygous deficiency
381 (*Df(2L)BSC148)* that deletes both NCad and CadN2 (*CadN[Df]/+; moody>ECad-RNAi*). The
382 reduction of both NCad genes strongly enhanced the ECad RNAi phenotypes (Fig. 7C-C") (n=10
383 larvae) with gaps or breaks within the SJ domain (yellow arrowheads) and aggregates of the

384 NrxIV::GFP protein (white arrowheads). The penetrance of the gaps or breaks present within the
385 SJs was significantly greater compared to control, ECad-RNAi alone or the ECad+NCad double
386 RNAi combination (Fig 7E). In summary these results suggest that ECad, NCad and CadN2 are
387 partially redundant in the peripheral glia.
388
389 *Dlg5 and cadherins function in the same pathway and underlie SJ and spot AJ formation*
390 The knockdown of ECad alone or in combination with loss of NCad specifically in the SPG
391 phenocopied the SJ phenotypes observed with the knockdown of Dlg5 and this led to the
392 hypothesis that these proteins might function in the same or parallel pathways. To test this, we
393 combined Dlg5 and ECad RNAi lines and assessed the effects of simultaneous knockdown on SJ
394 formation. We observed a strong enhancement of the ECad-RNAi phenotypes by Dlg5-RNAi
395 (Fig. 7D-D") (n=13 larvae) where the percentage of nerves affected with Dlg5+ECad-RNAi
396 were significantly greater than ECad-RNAi alone (n=6 larvae) and ECad+NCad-RNAi (Fig. 7E).
397 The effects of Dlg5+ECad-RNAi were on par with the severity and penetrance of we observed
398 with ECad-RNAi plus the heterozygous NCad+CadN2 deficiency. These results suggest that
399 Dlg5 and cadherin function synergistically in the SPG and that Dlg5 may play a role in SJ
400 formation.
401 We attempted to test the effects of Dlg5 knockdown on the formation of sAJ using
402 immunolabeling with ECad::cherry and NCad::cherry, however this analysis was difficult due to
403 the distribution of cadherin puncta within all three glial layers. To better assess the effects on
404 sAJ, we used TEM analysis of Dlg5-RNAi knockdown using the pan-glial driver (*repo>Dlg5-*
405 *RNAi, Dicer2*) and assessed for the presence of sAJ (Fig. 8). In controls (*repo>Dicer2*)(n=3
406 larvae) we observed sAJ between the multiple glial layers, specifically between the PG and SPG

407 (yellow) and between SPG and WG (green) with an average of 1.8 sAJ per section for each (Fig.
408 8E; red circles). We observed rare instances of sAJ between WG processes and found sAJ
409 between SPG only when two SPG where present (Fig. 8E). Knockdown of Dlg5 (*repo>Dlg5-*
410 *RNAi*) lead to a significant reduction in the sAJ between both the PG-SPG and the SPG-WG
411 membranes (on average 0.3 and 0.5 per section respectively) (Fig. 8A,B) (n=2 larvae). This was
412 similar to the loss of sAJ between the glial layers when ECad-RNAi was expressed (*repo>ECad-*
413 *RNAi, Dicer2*) (Fig. 8C,D) where the presence of sAJ decreased to an average of 0.1 between
414 PG-SPG and 0.3 between SPG-WG per section (n=5 larvae). Our data suggest that knockdown
415 of Dlg5 or ECad have the same effects resulting in a reduction in sAJs junctions between the
416 glial layers.
417
418 *Loss of Dlg5 and ECad disrupts the blood-brain barrier and larval locomotion*
419 Glial septate junctions form the blood-barrier in the Drosophila CNS and PNS. Given the strong
420 effects of loss of both Dlg5 and the Cadherins on the septate junctions, we next tested for
421 changes to the blood-brain barrier using a dextran dye assay (Fig. 9). Dye was blocked, as
422 expected, from entry into the brain lobes and ventral nerve cord of the CNS in controls (*moody-*
423 *GAL4*) (Fig. 9A) (n=30 larvae), while knockdown of NrxIV as a positive control (*moody>NrxIV-*
424 *RNAi*) disrupted the SJ and led to significant dye penetration (Fig. 9B, F) (n=2 larvae).
425 Knockdown of ECad but not Dlg5 lead to a small but significant increase in the penetration of
426 dye into the CNS (Fig. 9C,D,F) (n=72 and 53 larvae respectively) and the double knockdown of
427 Dlg5+ECad (*moody>Dlg5-RNAi, ECad-RNAi*) (n=70 larvae) had significantly more dye
428 penetration compared to either RNAi alone (Fig. 9E,F).

429 We wanted to determine if the changes to the glial layers, the septate junctions and the
430 disruption of the blood-brain barrier affected nervous system function. To this end, we measured
431 various parameters of locomotor behavior (Fig. 10) including the total distance and the average
432 speed at which 3rd instar larvae travelled. We found that in controls (*moody-GAL4* crossed to
433 *w[1118]*), larvae travelled on average a total distance of 67mm at an average speed of 1.12
434 mm/sec (Fig. 10A, F-G). We used the knockdown of NrxIV (*moody>NrxIV-RNAi*), which
435 disrupts SJs and the blood-barrier as a positive control and larvae motion was significantly
436 compromised (Fig. 10E-G). When compared to control larvae, both parameters were
437 significantly reduced after ECad knockdown (*moody>ECad-RNAi*)(Fig. 10C,F,G) and Dlg5
438 knockdown (*moody>Dlg5-RNAi*)(Fig.10B,F,G). The combined knockdown of Dlg5 and ECad
439 (*moody>ECad-RNAi, Dlg5-RNAi*) significantly reduced locomotion (Fig. 10D,F,G) compared to
440 ECad-RNAi or Dlg5-RNAi alone and matched the disruption in locomotion observed with
441 NrxIV-RNAi. Our results suggest that the disruption of the SJ domains leads to changes in the
442 integrity of the blood-brain barrier and to changes in animal locomotion.
443
444 **Discussion:**
445 Our aim was to discover PDZ domain scaffolding proteins that play a role in glial ensheathment
446 of peripheral axons. We identified that the MAGUK protein Discs-large 5 (Dlg5) has a role in
447 subperineurial glia and septate junction morphology. To investigate the role of Dlg5 further we
448 focused on cadherins and found that loss of N-Cadherin and E-Cadherin phenocopied the loss of
449 Dlg5 leading to gaps in the SPG and septate junctions. This leads to a model where Dlg5 plays a
450 role in conjunction with Cadherins in glial membrane stabilization and SJ formation in the
451 subperineurial glia.

452 Dlg5 performs multiple independent functions in both mammals and Drosophila including
453 regulation of cell proliferation, polarity, growth, and trafficking of junctional complexes and
454 these functions are highly context specific (Kwan et al., 2016; Liu et al., 2017; Venugopal et al.,
455 2020). One established function for Dlg5 is a role in polarity. In Drosophila, Dlg5 plays a role in
456 establishing apical-basal polarity in follicular epithelia, where Dlg5 localizes at the apical
457 membrane and adherens junction in early egg chambers and where loss of Dlg5 generates
458 epithelia polarity defects (Luo et al., 2016). In follicular epithelia, Dlg5 promotes the apical
459 membrane localization of Crumbs to establish polarity. Our data suggests that in the context of
460 glial cells, Dlg5 also may play a role in maintaining cell polarity as we observed changes to the
461 SJ and the distribution of Dlg and Scrib. However, unlike the follicular epithelial cells, Dlg5
462 most likely does not function through changes to Crumbs in the SPG as peripheral glia do not
463 express Crumbs and knockdown of Crumbs had no effect. Glial cells are likely polarized by a
464 different mechanism in a Crumbs independent manner. We also failed to detect Par-3 or Par-6 in
465 the peripheral glia and RNAi knockdown of these apical polarity proteins had no effect. The
466 unconventional polarization mechanism adopted by glia could be attributed to differences in the
467 architecture of glial cells compared to epithelia. We did find that Sdt, a component of the
468 Crumbs complex, is required in the peripheral glia, which raises the question as to whether Sdt
469 interacts with non-canonical partners to perform similar functions as seen in epithelial cells or
470 whether Sdt might have an entirely different and novel function in glial cells. The latter is more
471 likely as Sdt knockdown does not affect SJ morphology.
472 Another potential Dlg5 function could be through the interface between Cadherin function and
473 the glial cytoskeleton or in the assembly of spot adherens junctions. Dlg5 links the vinexin-
474 vinculin complex and beta-catenin at sites of cell-cell contact in mammalian fibroblasts and

475 epithelial cells (Wakabayashi et al., 2003). Loss of Dlg5 in the SPG resulted in the reduction in
476 the number of spot adherens junctions and enhanced the SPG defects generated by loss of
477 Cadherins. However, the degree of overlap between Dlg5 and Cadherins in the 3rd instar larvae
478 was not extensive suggesting a role of Dlg5 in the construction of the sAJs rather than the
479 maintenance and ongoing stability of these junctions. This mirrors prior observations where Dlg5
480 was necessary for the trafficking of N-cad/beta-catenin complexes to the membrane (Nechiporuk
481 et al., 2007).
482 It is possible that Dlg5 function with regards to junctional complexes is highly context
483 specific. In the Drosophila ovary, Dlg5 is found associated with basolateral SJ proteins
484 (including Dlg1, Neuroglian, ATPα and Lachesin) and to a smaller extent the AJ in border cells
485 (Luo et al., 2019), and Dlg5 was localized with Dlg1 in stage 10 follicular epithelia (Luo et al.,
486 2016). The loss of Dlg5 disrupted the distribution of Arm (beta-catenin) in border cells (Luo et
487 al., 2019) and E-Cadherin in follicular cells (Luo et al., 2016), yet had no effect on the
488 distribution of Dlg1 or the SJ protein Neuroglian (Luo et al., 2019). In wing discs, Dlg5 mutants
489 have a reduction of apical domain determinants but not a loss of cell polarity and a very specific
490 defect in the recruitment of N-Cadherin to adherens junctions but not E-Cadherin (Venugopal et
491 al., 2020). Our results shown that in the SPG, Dlg5 was not found associated with any junctional
492 complexes except with puncta of NCad and ECad, and was excluded from the SJ. As well loss of
493 Dlg5 resulted in the disruption of both sAJ and SJ morphology suggesting a global defect in cell
494 polarity rather than a specific disruption to a single junctional domain.
495 A third potential function for Dlg5 is in controlling cell proliferation (Nakamura et al., 1998; Liu
496 et al., 2017) where Dlg5-knockdown cells grow faster. Dlg5 function appears to be highly cell
497 specific as Dlg5 can function either as tumour suppressor or tumour enhancer in different cancer

498 cell lines (Andolfi et al., 2022) (Liu et al., 2014b). As SPG are polyploid cells and do not
499 undergo mitosis, we do not think the role of Dlg5 is to control SPG proliferation. However, the
500 SPG are very large cells and polyploidy is necessary for glial growth to match the expanding
501 CNS, and required for a functional blood–brain barrier (Unhavaithaya and Orr-Weaver, 2012). A
502 key component in the SPG size increase is the Hippo pathway (Liu et al., 2017), a key regulator
503 of organ size and tissue homeostasis in many tissues (Limmer et al., 2014; Yu et al., 2015; Li and
504 Guan, 2022). The Hippo pathway regulates the transcriptional regulator Yorkie specifically by
505 inactivating Yorkie through phosphorylation and degradation (Comoletti et al., 2003). In
506 Drosophila, Yorkie is necessary for normal glial cell numbers and expansion (Reddy and Irvine,
507 2011), and for the extensive growth of SPG (Li et al., 2017). Loss of Yorkie activity in the SPG
508 causes abnormal endoreplication, defective septate junctions and BBB disruption (Li et al.,
509 2017). There is evidence that Dlg5 can indirectly regulate Hippo signaling in multiple
510 Drosophila tissues, where loss of Dlg5 leads to activation of Hippo signaling and the repression
511 of Yorkie (Kwan et al., 2016; Kaya-Copur et al., 2021; Venugopal et al., 2020). Our results
512 found that loss of Dlg5 and Cadherins leads to SJ and BBB disruption suggesting that, if Hippo
513 is involved, in the SPG loss of Dlg5 leads to a decrease in Yorkie activity and an increase in
514 Hippo signaling. Given that the polypoid SPG do not divide but rather grow in size, it is possible
515 that loss of Dlg5 leads to reduced growth in SPG which manifests as hole-like structures in the
516 SPG and the SJ. However, whether Dlg5 regulates SPG and SJ development through Hippo
517 pathway or other pathways remains to be elucidated.
518
519 **Figures**
520
521 **Figure 1:** Identification of PDZ proteins required in glial cells of the peripheral nerve.

522 **A:** Summary of PDZ protein RNAi screen. Details of RNAi lines used to target each candidate
523 gene can be found in Table 1. Each box represents an individual RNAi line with green meaning
524 wild type and magenta representing abnormal glial phenotypes.
525 **B-G:** Longitudinal sections of peripheral nerves from control and selections of positive candidate
526 identified in the RNAi screen. All glial membranes labeled with mCD8::RFP (green) and axons
527 immunolabeled with anti-Futsch (22C10; magenta). The pan-glial driver repo-GAL4 was used
528 and crossed to:
529 (B-B") Control (*w[1118]*) peripheral nerve.
530 (C-C") Rho-GEF2-RNAi. Swollen regions are indicated (C', yellow arrowheads) and these
531 swellings were accompanied by defasciculation of the axons in that region (white arrowheads,
532 C'').
533 (D-D") Dlg1-RNAi. Glial membranes were disrupted (D', yellow arrowhead).
534 (E-E") Scrib-RNAi. Glial membranes were abnormal with accumulations (E', yellow
535 arrowhead).
536 (F-F") Loco-RNAi. Peripheral nerves were swollen and vacuole-like structures were observed
537 within the glial membranes (F', yellow arrowheads).
538 (G-G") Dlg5-RNAi. Peripheral nerves had disrupted inner glial membranes (G', yellow
539 arrowheads). The morphology of axons in these nerves were unaffected (G'').
540 Scale bars: 15µm
541
542
543 **Figure 2.** Knockdown of Dlg5 in the peripheral glial leads to disruptions of the SPG and WG.
544 **A-B:** Endogenously tagged Dlg5 (Dlg5::GFP, green) reveals expression within glia and axons in
545 the PNS. All glial membranes labeled with mCD8::RFP (repo-GAL4, magenta)(A) or with axons
546 immunolabeled with anti-Futsch (22C10, magenta)(B).
547 **C-D:** Perineurial glia. The PG driver 46F-GAL4 crossed to w[1118] (C) or Dlg5-RNAi (D). The
548 PG membranes (mCD8::RFP, green) and axons (magenta) in both appeared normal in
549 longitudinal and cross sections.
550 **E-F**: Subperineurial glia. The SPG driver Gli-GAL4 crossed to w[1118]( E) or Dlg5-RNAi (F)
551 SPG membranes were labeled with mCD8::RFP (green) and WG membranes with Nrv2::GFP
552 (magenta). The SPG membrane in control (**E'**) was continuous along the length of the nerve. In
553 Dlg5-RNAi nerves (**G'**), the SPG was disrupted with breaks/gaps in the membrane (yellow
554 arrowheads). The WG in both control (E'') and Dlg5-RNAi (G'') nerves extended normal
555 processes along the length of the nerve. An SPG nuclei (asterisk) is indicated.
556 **G-H**: Wrapping glia. The WG driver Nrv2-GAL4 crossed to w[1118] (G) and Dlg5-RNAi (**H**).
557 The WG membranes were labeled with mCD8::RFP (green) and axons labeled with anti-Futsch
558 (22C10, magenta). WG in control nerves (G") extended normal processes along the length of the
559 nerve and in cross-sections surrounded the axons (magenta). WG in Dlg5-RNAi nerves had
560 fewer and disrupted processes (H", yellow arrowheads). In cross-sections the WG processes did
561 not extend around the axons (yellow arrowhead).
562 Scale bars: 15µm
563
564
565 **Figure 3.** Knockdown of Dlg5 in the SPG disrupts septate junction and membrane morphology.
566 The SPG drivers Gli-GAL4 (A-C) or SPG-GAL4 (E,F) driving mCD8::RFP (magenta) crossed
567 to control (w[1118]) or Dlg5-RNAi. Scale bars: 15µm

568 **A-B:** Gli-GAL4 with NrxIV::GFP. Control (**A**) and Dlg5-RNAi (**B**) peripheral nerves with the
569 SPG membrane labeled with mCD8::RFP (magenta) and SJs labelled with NrxIV::GFP (green).
570 The SJs (**A'**) and SPG membranes (A") were continuous. In *Dlg5-RNAi* nerves SJ strands were
571 disrupted (B'), which corresponded to the disruptions in the SPG membrane (B" yellow
572 arrowheads).
573 **C-D:** Gli-GAL4. Control (**A**) and Dlg5-RNAi (**B**) peripheral nerves with the SPG membrane
574 labeled with mCD8::RFP (magenta) and SJs immunolabelled for Nrv2.1 (green. The SJs (C')
575 and SPG membranes (C") were continuous. In Dlg5-RNAi nerves SJ strands were disrupted
576 (D''), which corresponded to the disruptions in the SPG membrane (B" yellow arrowheads).
577 **E:** SPG-GAL4, NrxIV::GFP. Dicer 2 enhanced the *Dlg5-RNAi phenotypes where* NrxIV and SJs
578 formed accumulations (**E'**), which corresponded to accumulations and disruption in the SPG
579 membrane (E" yellow arrowheads).
580 **F:** Quantification of the SJ disruptions. The number of nerves per animal with disrupted SJs
581 were quantified for SPG-GAL4 crossed to w[1118] (control) and Dlg5-RNAi or Dicer2 and
582 Dicer2, Dlg5-RNAi. The mean and standard deviation are indicated. Statistical significance was
583 determined by one-way ANOVA with Tukey's *post hoc* multiple comparison test for each group
584 (*$p \leq 0.5$, **** $p \leq 0.0001$)
585
586
587 **Figure 4.** N-Cadherin and E-Cadherin are expressed in glial cells of the larval peripheral nerve
588 **A-B**: Control 3rd instar peripheral nerves with NCad::mCherry (magenta, A,A") and
589 ECad::cherry (magenta, B,B"). The glial membranes were labeled with mCD8::GFP (green).
590 Both Cadherins were distributed throughout the nerve indicated in the cross-sections of each
591 peripheral nerve (yellow arrowheads).
592 **C:** Longitudinal sections of peripheral nerves with NCad::mCherry (magenta, C,C') and
593 ECad::GFP (green, C,C"). Some but not all NCad overlaps with ECad puncta (yellow
594 arrowheads).
595 **D,E:** TEM analysis of control (repo-GAL4) nerve with the three glial layers falsed coloured:
596 WG (green), SPG (magenta), PG (cyan). Spot adherens junctions are indicated (red circles).
597 Scale bars: 1 µm
598 **F,G:** Longitudinal sections of peripheral nerves with Dlg5::GFP (green) and NCad::mCherry
599 (magenta, F,F') and ECad::mCherry (magenta, G,G'). Some but not all Dlg5 overlaps NCad and
600 ECad puncta (yellow arrowheads).
601 Scale bars: 15µm
602
603
604 **Figure 5.** Knockdown of ECad in the WG and SPG affects glial morphology.
605 **A-B**: All glia. repo-GAL4 crossed to Dicer2 (control) (A) and ECad-RNAi, Dicer2 (B)
606 Peripheral nerves with all glial membranes labeled with mCD8::GFP (green). SJ were
607 immunolabeled with Dlg1 (magenta). Glial membranes (A') and a linear SJ (A") extends along
608 the length of the nerve in control. With ECad-RNAi, glial membranes are disrupted (yellow
609 arrowheads, B,B') and vacuole-like or hole-like structures observed (white arrowheads, B'B")
610 and the SJ disorganized.
611 **C-D**: Wrapping glia. Nrv2-GAL4 crossed to Dicer2 (control)(C) and ECad, Dicer2 (D).
612 Longitudinal sections of peripheral nerves with WG membranes labeled with mCD8::GFP
613 (green) and axons immunolabeled with anti-Futsch (22C10, magenta). The WG membranes

614 continuously extend along the length of control (green, C,C'). With ECad-RNAi, WG
615 membranes were discontinuous and disrupted (yellow arrowheads, D,D'). The axon morphology
616 in ECad-RNAi peripheral nerves looked similar to controls (magenta, D,D'').
617 **E-F**: Subperineurial glia. Gli-GAL4 crossed to Dicer 2 (control)(E) and ECad-RNAi, Dicer2 (F)
618 with the SPG membrane labeled with mCD8::RFP (magenta) and the SJ immunolabeled with
619 Dlg1 (green). The SPG membrane is continuous along the length of control (magenta, E") and
620 the SJ forms a continuous line (E'). In ECad-RNAi nerves the membrane was discontinuous and
621 disrupted (yellow arrowheads, F") and whereas Dlg1 was lost in regions of the nerve where the
622 SPG membrane was disrupted. Scale bars: 15µm
623
624
625 **Figure 6.** Knockdown of ECad in the SPG disrupts the septate junctions.
626 Longitudinal sections of 3rd instar peripheral nerves with the SPG driver, moody-GAL4 driving
627 mCD8::RFP (magenta) to label the glial membranes and with NrxIV::GFP (green) to mark the
628 SJ. Scale bars: 15µm
629 **A:** Control. Moody-GAL4 crossed to w[1118]. Glial membranes (A") and a linear SJ (A')
630 extends along the length of the nerve in control.
631 **B:** Quantification of the ECad-RNAi effects on the SJ. The percentage of nerves affected per
632 larvae were determined for each genotype. The mean and standard deviation are indictated.
633 Statistical significance was determined by one-way ANOVA with Tukey's *post hoc* multiple
634 comparison test for each RNAi compared to the control (**** $p \leq 0.0001$).
635 **C-D**: ECad-RNAi. Moody-GAL4 crossed with ECad-RNAi. The SJ and glial membranes
636 contained breaks or holes in the immunolabeling (yellow arrowheads). D represents a digital
637 magnification (200%) of C to highlight the membrane and SJ breaks.
638 **E-F**: ECad-RNAi plus Dicer2. Moody-GAL4 crossed with ECad-RNAi and Dicer2 to enhance
639 the RNAi efficiency. NrxIV formed aggregates in the membrane which appeared collapsed
640 (yellow arrowheads). F represents a digital magnification (200%) of E to highlight the NrxIV
641 aggregates.
642
643
644 **Figure 7.** Knockdown of Dlg5, ECad and NCad disrupts septate junctions.
645 Longitudinal sections of 3rd instar peripheral nerves with the SPG driver, moody-GAL4 driving
646 mCD8::RFP (magenta) to label the glial membranes and with NrxIV::GFP (green) to mark the
647 SJ. Scale bars: 15µm
648 **A:** Control. Moody-GAL4 crossed to w[1118]. Glial membranes (A") and a linear SJ (A')
649 extends along the length of the nerve in control.
650 **B**: NCad-RNAi, CadN2-RNAi. Moody-GAL4 crossed with NCad-RNAi, CadN2-RNAi. The SJ
651 (B') and glial membranes (B") contained breaks or holes (yellow arrowheads).
652 **C**: ECad-RNAi, CadN-Df/+. Moody-GAL4 crossed with ECad-RNAi and a deficiency that
653 uncovers both NCad and CadN2. NrxIV formed aggregates (C') and those corresponded to
654 membrane concentrations (white arrowhead). Disrupted of the SJ occurred in the same places as
655 loss or holes in the glial membrane (yellow arrowheads).
656 **D:** Dlg5-RNAi, ECad-RNAi. Moody-GAL4 crossed with Dlg5 and ECad-RNAi. NrxIV formed
657 aggregates (C') and those corresponded to membrane concentrations (white arrowhead). SJ were
658 reduced and large holes were observed in the glial membranes (yellow arrowheads).

659 **E:** Quantification of the RNAi effects on the SJ. The percentage of nerves affected per larvae
660 were determined for each genotype. The mean and standard deviation are indicated. Statistical
661 significance was determined by one-way ANOVA with Tukey's *post hoc* multiple comparison
662 test for each RNAi compared across multiple genotypes. p values compared to control are
663 indicated above each genotype. (*$p \leq 0.5$, **$p \leq 0.01$, *** $p \leq 0.001$, **** $p \leq 0.0001$, non-
664 significant differences are not indicated)
665
666
667 **Figure 8.** Knockdown of Dlg5 and ECad leads to loss of spot adherens junctions**.**
668 Transmission electron microscope images of repo-GAL crossed to Dlg5-RNAi (A-B), ECad-
669 RNAi (C-D) or w1118 (E) with the SPG and WG layers false coloured (SPG: magenta; WG:
670 green). The outer PG layer and the inner axons are not coloured. Spot adherens junctions are
671 indicated with a red circle. Unusual gaps within the SPG or between the SPG and WG are
672 indicated with an asterisk (red). Scale bars: 1 µm.
673 F: Quantification of the number of spot adherens junctions identified between the PG and SPG
674 membranes and the SPG and WG membranes. The mean and standard deviation are indicated.
675 Statistical significance was determined by one-way ANOVA with Tukey's *post hoc* multiple
676 comparison test for each group compared to control (**** $p \leq 0.0001$)
677
678
679 **Figure 9:** Knockdown of Dlg5 and ECad impairs blood-brain barrier integrity.
680 **A-D:** Fire LUT showing blood-brain permeability assay using moody-
681 GAL4>mCD8::GFP crossed to w[1118] (control)(A), Dlg5-RNAi (B), ECad-RNAi (C), Dlg5-
682 RNAi, ECad-RNAi (D) or NrxIV-RNAi (E). White arrows highlight regions of significant dye
683 labeling of the neuropile. Scale bars: 150 µm.
684 **F:** Quantification of mean fluorescent intensity inside the brain lobe. The mean and standard
685 deviation are indicated. Dye penetration for NrxIV-RNAi was determined at a lower laser
686 intensity than the other genotypes. Statistical significance was determined by one-way ANOVA
687 with Tukey's *post hoc* multiple comparison test for each group (*$p \leq 0.5$, **$p \leq 0.01$,
688 *** $p \leq 0.001$, **** $p \leq 0.0001$, non-significant differences are not indicated).
689
690
691 **Figure 10.** Loss of Dlg5 and ECad in the SPG impairs animal locomotion
692 **A-E**: Movement trajectories of 3rd instar larvae from moody-GAL4 flies crossed with w[1118]
693 (A), Dlg5-RNAi (B), ECad-RNAi (C), Dlg5-RNAi, ECad-RNAi (D), and NrxIV-RNAi (E).
694 Scale bars: 10 mm.
695 **F-G**: Comparison of average speed (F) and total travel distance (G) of moody-GAL4 driving
696 Dlg5-RNAi, ECad-RNAi, Dlg5+ECad-RNAi, NrxIV-RNAi and control, w[1118]. The mean and
697 standard deviation are indicated. Statistical significance was determined by one-way ANOVA
698 with Tukey's *post hoc* multiple comparison test for each group (*$p \leq 0.5$, **$p \leq 0.01$,
699 *** $p \leq 0.001$, **** $p \leq 0.0001$, non-significant differences are not indicated).
700
701
702
703

704 **References:**
705
706 Andolfi C, Tiribelli C, Pascut D (2022) Recent Hints on the Dual Role of Discs Large MAGUK
707 Scaffold Protein 5 in Cancers and in Hepatocellular Carcinoma. Front Biosci (Landmark
708 Ed) 27:164.
709 Aranjuez G, Kudlaty E, Longworth MS, McDonald JA (2012) On the role of PDZ domain-
710 encoding genes in Drosophila border cell migration. G3 2:1379-1391.
711 Auld VJ, Fetter RD, Broadie K, Goodman CS (1995) Gliotactin, a novel transmembrane protein
712 on peripheral glia, is required to form the blood-nerve barrier in Drosophila. Cell 81:757-
713 767.
714 Bao L, Samuels S, Locovei S, Macagno ER, Muller KJ, Dahl G (2007) Innexins form two types
715 of channels. FEBS letters 581:5703-5708.
716 Baumgartner S, Littleton JT, Broadie K, Bhat MA, Harbecke R, Lengyel JA, Chiquet-Ehrismann
717 R, Prokop A, Bellen HJ (1996) A Drosophila neurexin is required for septate junction and
718 blood-nerve barrier formation and function. Cell 87:1059-1068.
719 Bhat MA (2003) Molecular organization of axo-glial junctions. Curr Opin Neurobiol 13:552-
720 559.
721 Brooks DS, Vishal K, Kawakami J, Bouyain S, Geisbrecht ER (2016) Optimization of wrMTrck
722 to monitor Drosophila larval locomotor activity. J Insect Physiol 93-94:11-17.
723 Brower DL (1984) Posterior-to-anterior transformation in engrailed wing imaginal disks of
724 Drosophila. Nature 310:496-497.
725 Buszczak M, Paterno S, Lighthouse D, Bachman J, Planck J, Owen S, Skora AD, Nystul TG,
726 Ohlstein B, Allen A, Wilhelm JE, Murphy TD, Levis RW, Matunis E, Srivali N, Hoskins
727 RA, Spradling AC (2007) The carnegie protein trap library: a versatile tool for
728 Drosophila developmental studies. Genetics 175:1505-1531.
729 Chen S, Rio C, Ji RR, Dikkes P, Coggeshall RE, Woolf CJ, Corfas G (2003) Disruption of ErbB
730 receptor signaling in adult non-myelinating Schwann cells causes progressive sensory
731 loss. Nat Neurosci 6:1186-1193.
732 Comoletti D, Flynn R, Jennings LL, Chubykin A, Matsumura T, Hasegawa H, Sudhof TC,
733 Taylor P (2003) Characterization of the interaction of a recombinant soluble neuroligin-1
734 with neurexin-1beta. J Biol Chem 278:50497-50505.
735 Dietzl G, Chen D, Schnorrer F, Su KC, Barinova Y, Fellner M, Gasser B, Kinsey K, Oppel S,
736 Scheiblauer S, Couto A, Marra V, Keleman K, Dickson BJ (2007) A genome-wide
737 transgenic RNAi library for conditional gene inactivation in Drosophila. Nature 448:151-
738 156.
739 Griffin JW, Thompson WJ (2008) Biology and pathology of nonmyelinating Schwann cells. Glia
740 56:1518-1531.
741 Harris BZ, Lim WA (2001) Mechanism and role of PDZ domains in signaling complex
742 assembly. J Cell Sci 114:3219-3231.
743 Humbert P, Russell S, Richardson H (2003) Dlg, Scribble and Lgl in cell polarity, cell
744 proliferation and cancer. Bioessays 25:542-553.
745 Kaya-Copur A, Marchiano F, Hein MY, Alpern D, Russeil J, Luis NM, Mann M, Deplancke B,
746 Habermann BH, Schnorrer F (2021) The Hippo pathway controls myofibril assembly and
747 muscle fiber growth by regulating sarcomeric gene expression. Elife 10.

748 Kelso RJ, Buszczak M, Quinones AT, Castiblanco C, Mazzalupo S, Cooley L (2004) Flytrap, a
749 database documenting a GFP protein-trap insertion screen in Drosophila melanogaster.
750 Nucleic Acids Research 32:D418-D420.
751 Kwan J, Sczaniecka A, Heidary Arash E, Nguyen L, Chen C-C, Ratkovic S, Klezovitch O,
752 Attisano L, McNeill H, Emili A, Vasioukhin V (2016) DLG5 connects cell polarity and
753 Hippo signaling protein networks by linking PAR-1 with MST1/2. Genes &
754 Development 30:2696-2709.
755 Lee T, Luo L (1999) Mosaic analysis with a repressible cell marker for studies of gene function
756 in neuronal morphogenesis. Neuron 22:451-461.
757 Li D, Liu Y, Pei C, Zhang P, Pan L, Xiao J, Meng S, Yuan Z, Bi X (2017) miR-285-Yki/Mask
758 double-negative feedback loop mediates blood-brain barrier integrity in Drosophila.
759 Proceedings of the National Academy of Sciences of the United States of America
760 114:E2365-E2374.
761 Li FL, Guan KL (2022) The two sides of Hippo pathway in cancer. Semin Cancer Biol 85:33-42.
762 Limmer S, Weiler A, Volkenhoff A, Babatz F, Klambt C (2014) The Drosophila blood-brain
763 barrier: development and function of a glial endothelium. Front Neurosci 8:365.
764 Liu J, Li J, Ren Y, Liu P (2014a) DLG5 in cell polarity maintenance and cancer development.
765 International journal of biological sciences 10:543-549.
766 Liu J, Li J, Ren Y, Liu P (2014b) DLG5 in cell polarity maintenance and cancer development.
767 Int J Biol Sci 10:543-549.
768 Liu J, Li J, Li PP, Wang YC, Liang ZY, Jiang YN, Li J, Feng C, Wang RQ, Chen H, Zhou C,
769 Zhang JM, Yang J, Liu PJ (2017) Loss of DLG5 promotes breast cancer malignancy by
770 inhibiting the Hippo signaling pathway. Scientific reports 7.
771 Luo J, Zhou P, Guo X, Wang D, Chen J (2019) The polarity protein Dlg5 regulates collective
772 cell migration during Drosophila oogenesis. PLoS One 14:e0226061.
773 Luo J, Wang H, Kang D, Guo X, Wan P, Wang D, Chen J (2016) Dlg5 maintains apical polarity
774 by promoting membrane localization of Crumbs during Drosophila oogenesis. Scientific
775 reports 6:26553.
776 Matzat T, Sieglitz F, Kottmeier R, Babatz F, Engelen D, Klambt C (2015) Axonal wrapping in
777 the Drosophila PNS is controlled by glia-derived neuregulin homolog Vein. Development
778 142:1336-1345.
779 Morin X, Daneman R, Zavortink M, Chia W (2001) A protein trap strategy to detect GFP-tagged
780 proteins expressed from their endogenous loci in Drosophila. Proc Natl Acad Sci U S A
781 98:15050-15055.
782 Nakamura H, Sudo T, Tsuiki H, Miyake H, Morisaki T, Sasaki J, Masuko N, Kochi M, Ushio Y,
783 Saya H (1998) Identification of a novel human homolog of the Drosophila dlg, P-dlg,
784 specifically expressed in the gland tissues and interacting with p55. FEBS Lett 433:63-
785 67.
786 Nechiporuk T, Fernandez TE, Vasioukhin V (2007) Failure of epithelial tube maintenance causes
787 hydrocephalus and renal cysts in Dlg5-/- mice. Developmental cell 13:338-350.
788 Nussbaum-Krammer CI, Neto MF, Brielmann RM, Pedersen JS, Morimoto RI (2015)
789 Investigating the spreading and toxicity of prion-like proteins using the metazoan model
790 organism C. elegans. J Vis Exp:52321.
791 Prakash S, Caldwell JC, Eberl DF, Clandinin TR (2005) Drosophila N-cadherin mediates an
792 attractive interaction between photoreceptor axons and their targets. Nature neuroscience
793 8:443-450.

794 Reddy BV, Irvine KD (2011) Regulation of Drosophila glial cell proliferation by Merlin-Hippo
795 signaling. Development 138:5201-5212.
796 Reilly E, Changela N, Naryshkina T, Deshpande G, Steward R (2015) Discs large 5, an Essential
797 Gene in Drosophila, Regulates Egg Chamber Organization. G3-Genes Genomes Genetics
798 5:943-952.
799 Sarov M et al. (2016) A genome-wide resource for the analysis of protein localisation in
800 Drosophila. eLife 5:e12068.
801 Schwabe T, Bainton RJ, Fetter RD, Heberlein U, Gaul U (2005) GPCR signaling is required for
802 blood-brain barrier formation in drosophila. Cell 123:133-144.
803 Sepp KJ, Auld VJ (1999) Conversion of lacZ enhancer trap lines to GAL4 lines using targeted
804 transposition in Drosophila melanogaster. Genetics 151:1093-1101.
805 Sepp KJ, Schulte J, Auld VJ (2000) Developmental dynamics of peripheral glia in Drosophila
806 melanogaster. Glia 30:122-133.
807 Sepp KJ, Schulte J, Auld VJ (2001) Peripheral glia direct axon guidance across the CNS/PNS
808 transition zone. Developmental biology 238:47-63.
809 Smendziuk CM, Messenberg A, Vogl AW, Tanentzapf G (2015) Bi-directional gap junction-
810 mediated soma-germline communication is essential for spermatogenesis. Development
811 142:2598-U2111.
812 Subbaiah VK, Kranjec C, Thomas M, Banks L (2011) PDZ domains: the building blocks
813 regulating tumorigenesis. The Biochemical journal 439:195-205.
814 Sun BH, Xu PZ, Salvaterra PM (1999) Dynamic visualization of nervous system in live
815 Drosophila. Proceedings of the National Academy of Sciences of the United States of
816 America 96:10438-10443.
817 Tonikian R, Zhang Y, Sazinsky SL, Currell B, Yeh JH, Reva B, Held HA, Appleton BA,
818 Evangelista M, Wu Y, Xin X, Chan AC, Seshagiri S, Lasky LA, Sander C, Boone C,
819 Bader GD, Sidhu SS (2008) A specificity map for the PDZ domain family. PLoS biology
820 6:e239.
821 Unhavaithaya Y, Orr-Weaver TL (2012) Polyploidization of glia in neural development links
822 tissue growth to blood-brain barrier integrity. Genes Dev 26:31-36.
823 Venken KJ, Schulze KL, Haelterman NA, Pan H, He Y, Evans-Holm M, Carlson JW, Levis RW,
824 Spradling AC, Hoskins RA, Bellen HJ (2011) MiMIC: a highly versatile transposon
825 insertion resource for engineering Drosophila melanogaster genes. Nat Methods 8:737-
826 743.
827 Venugopal P, Veyssiere H, Couderc JL, Richard G, Vachias C, Mirouse V (2020) Multiple
828 functions of the scaffold protein Discs large 5 in the control of growth, cell polarity and
829 cell adhesion in Drosophila melanogaster. BMC Dev Biol 20:10.
830 Vincent JB, Kolozsvari D, Roberts WS, Bolton PF, Gurling HM, Scherer SW (2004) Mutation
831 screening of X-chromosomal neuroligin genes: no mutations in 196 autism probands. Am
832 J Med Genet 129B:82-84.
833 Wakabayashi M, Ito T, Mitsushima M, Aizawa S, Ueda K, Amachi T, Kioka N (2003)
834 Interaction of lp-dlg/KIAA0583, a membrane-associated guanylate kinase family protein,
835 with vinexin and beta-catenin at sites of cell-cell contact. J Biol Chem 278:21709-21714.
836 Wang SH, Celic I, Choi SY, Riccomagno M, Wang Q, Sun LO, Mitchell SP, Vasioukhin V,
837 Huganir RL, Kolodkin AL (2014) Dlg5 regulates dendritic spine formation and
838 synaptogenesis by controlling subcellular N-cadherin localization. The Journal of
839 neuroscience : the official journal of the Society for Neuroscience 34:12745-12761.

840 Xie X, Auld VJ (2011) Integrins are necessary for the development and maintenance of the glial
841 layers in the Drosophila peripheral nerve. Development 138:3813-3822.
842 Yonekura S, Xu L, Ting CY, Lee CH (2007) Adhesive but not signaling activity of Drosophila
843 N-cadherin is essential for target selection of photoreceptor afferents. Developmental
844 biology 304:759-770.
845 Yu FX, Zhao B, Guan KL (2015) Hippo Pathway in Organ Size Control, Tissue Homeostasis,
846 and Cancer. Cell 163:811-828.
847

Figure 1

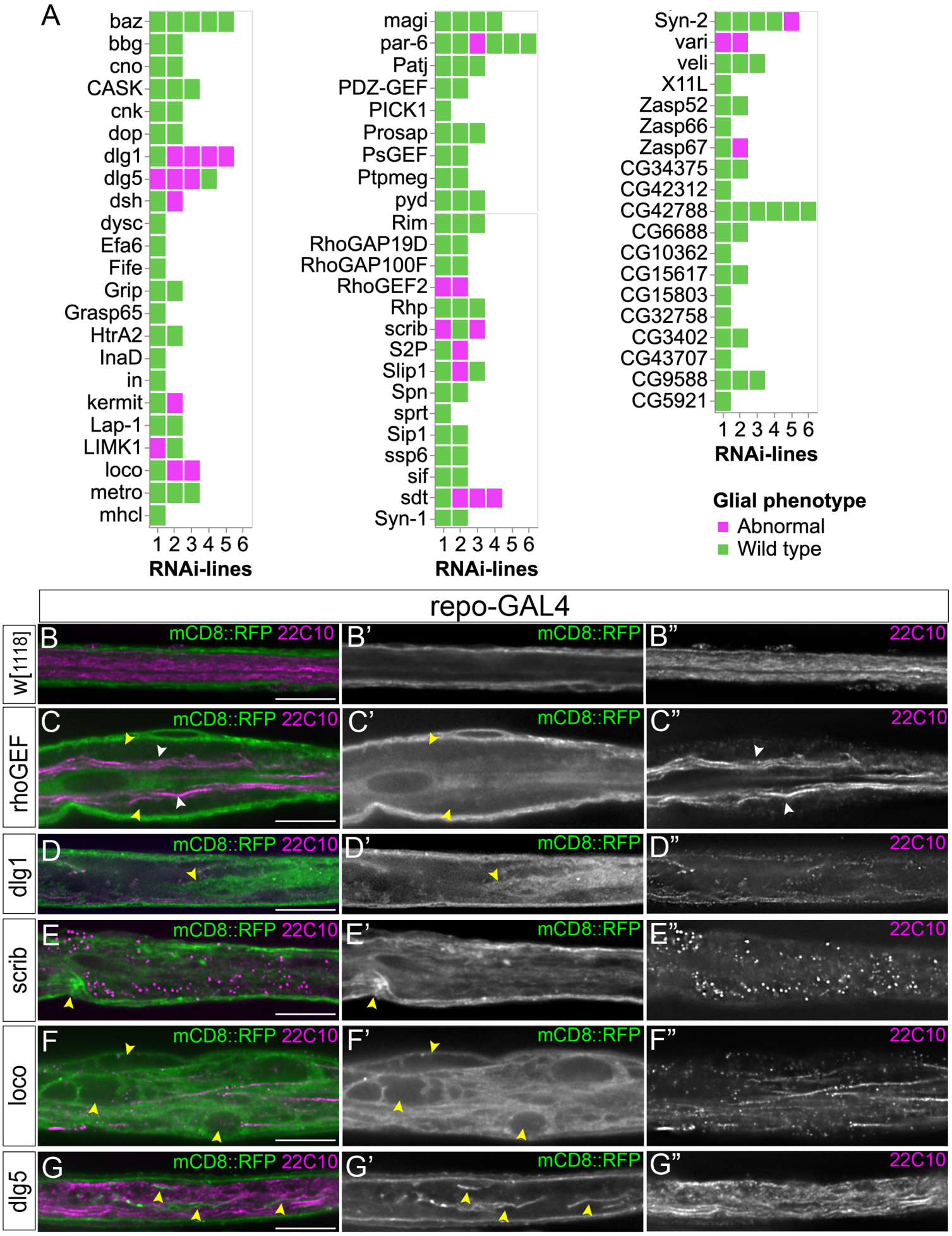
A
baz
bbg
cno
CASK
cnk
dop
dlg1
dlg5
dsh
dysc
Efa6
Fife
Grip
Grasp65
HtrA2
InaD
in
kermit
Lap-1
LIMK1
loco
metro
mhcl
1 2 3 4 5 6
RNAi-lines
magi
par-6
Patj
PDZ-GEF
PICK1
Prosap
PsGEF
Ptpmeg
pyd
Rim
RhoGAP19D
RhoGAP100F
RhoGEF2
Rhp
scrib
S2P
Slip1
Spn
sprt
Sip1
ssp6
sif
sdt
Syn-1
1 2 3 4 5 6
RNAi-lines
Syn-2
vari
veli
X11L
Zasp52
Zasp66
Zasp67
CG34375
CG42312
CG42788
CG6688
CG10362
CG15617
CG15803
CG32758
CG3402
CG43707
CG9588
CG5921
1 2 3 4 5 6
RNAi-lines
Glial phenotype
Abnormal
Wild type
repo-GAL4
w[1118]
rhoGEF
dlg1
scrib
loco
dlg5
B mCD8::RFP 22C10
B' mCD8::RFP
B" 22C10
C mCD8::RFP 22C10
C' mCD8::RFP
C" 22C10
D mCD8::RFP 22C10
D' mCD8::RFP
D" 22C10
E mCD8::RFP 22C10
E' mCD8::RFP
E" 22C10
F mCD8::RFP 22C10
F' mCD8::RFP
F" 22C10
G mCD8::RFP 22C10
G' mCD8::RFP
G" 22C10

# Figure 2

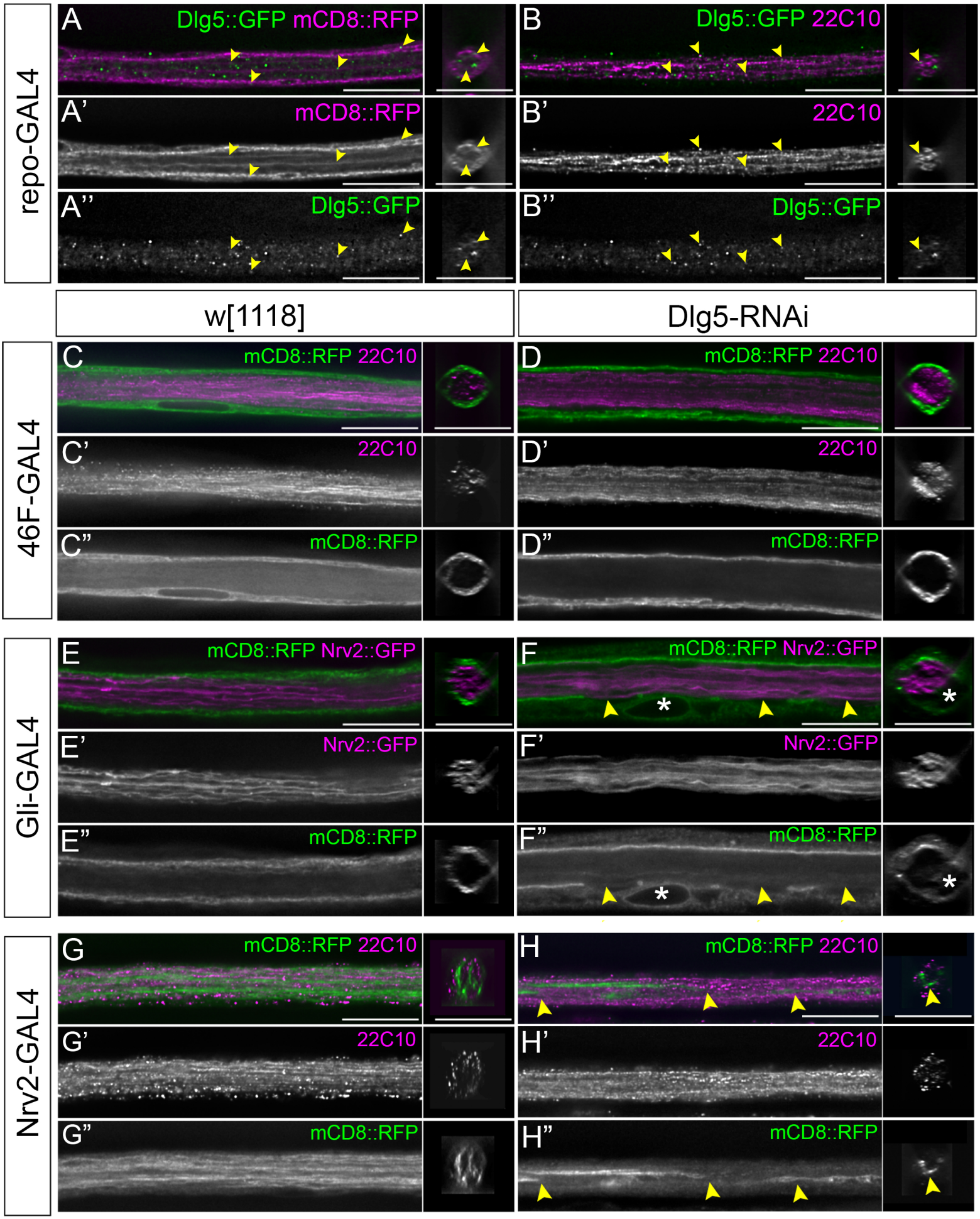
repo-GAL4
A
Dlg5::GFP mCD8::RFP
A'
mCD8::RFP
A''
Dlg5::GFP
B
Dlg5::GFP 22C10
B'
22C10
B''
Dlg5::GFP
w[1118]
Dlg5-RNAi
46F-GAL4
C
mCD8::RFP 22C10
C'
22C10
C''
mCD8::RFP
D
mCD8::RFP 22C10
D'
22C10
D''
mCD8::RFP
Gli-GAL4
E
mCD8::RFP Nrv2::GFP
E'
Nrv2::GFP
E''
mCD8::RFP
F
mCD8::RFP Nrv2::GFP
F'
Nrv2::GFP
F''
mCD8::RFP
Nrv2-GAL4
G
mCD8::RFP 22C10
G'
22C10
G''
mCD8::RFP
H
mCD8::RFP 22C10
H'
22C10
H''
mCD8::RFP

# Figure 3

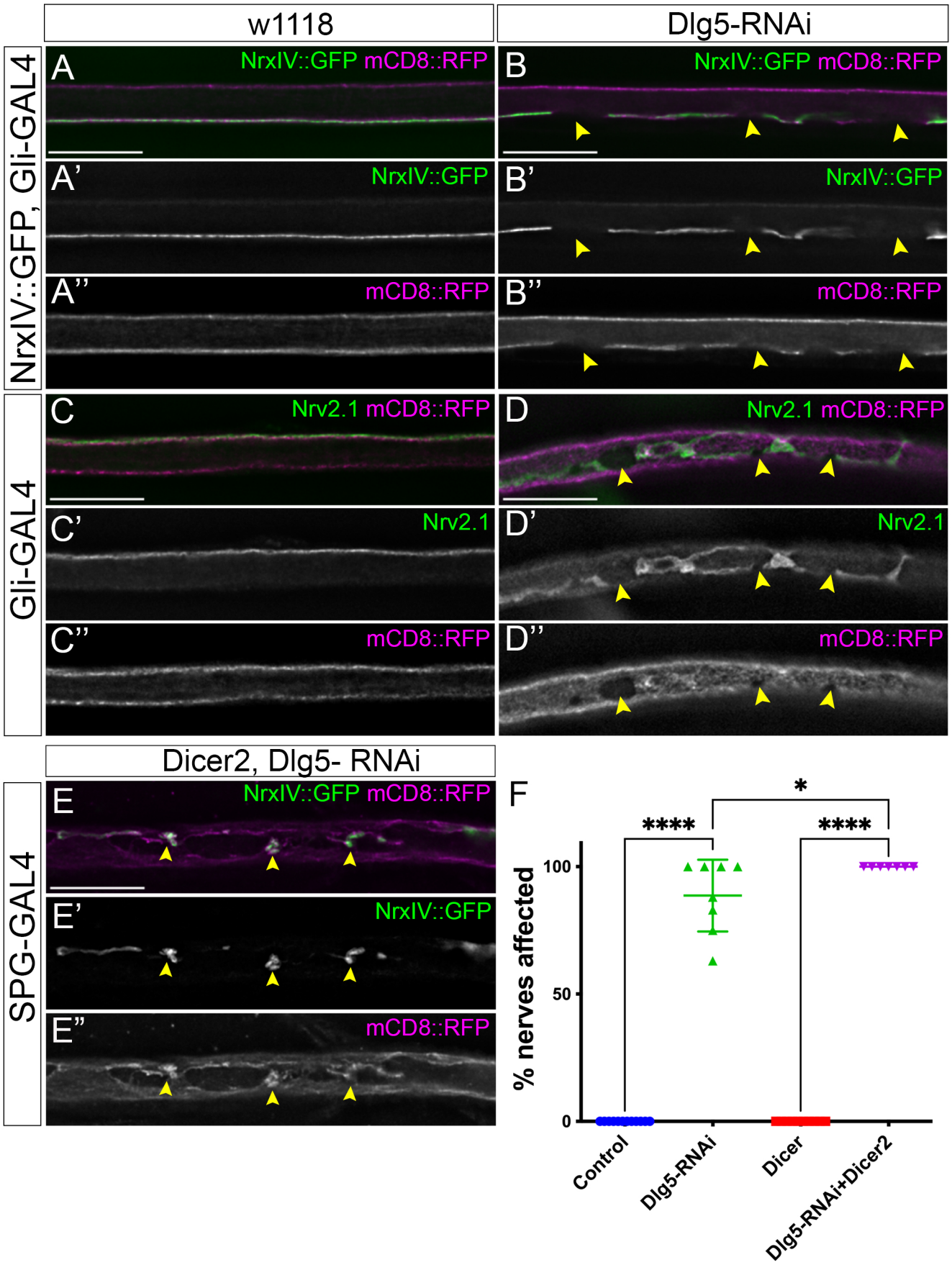
w1118
Dlg5-RNAi
NrxIV::GFP, Gli-GAL4
Gli-GAL4
A
NrxIV::GFP mCD8::RFP
A'
NrxIV::GFP
A''
mCD8::RFP
B
NrxIV::GFP mCD8::RFP
B'
NrxIV::GFP
B''
mCD8::RFP
C
Nrv2.1 mCD8::RFP
C'
Nrv2.1
C''
mCD8::RFP
D
Nrv2.1 mCD8::RFP
D'
Nrv2.1
D''
mCD8::RFP
Dicer2, Dlg5- RNAi
SPG-GAL4
E
NrxIV::GFP mCD8::RFP
E'
NrxIV::GFP
E''
mCD8::RFP
F
% nerves affected
100
50
0
****
*
****
Control
Dlg5-RNAi
Dicer
Dlg5-RNAi+Dicer2

# Figure 4

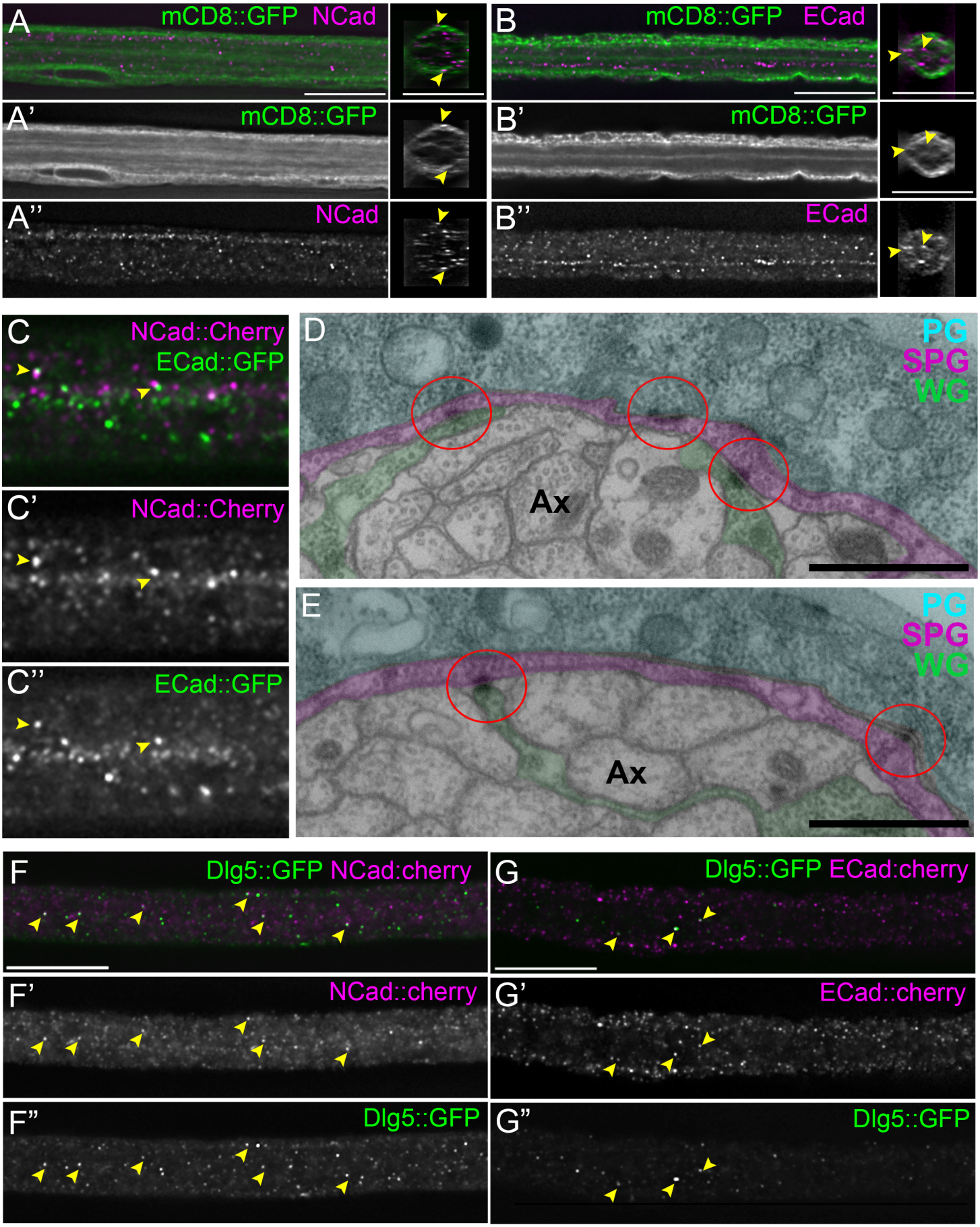
A
mCD8::GFP NCad
B
mCD8::GFP ECad
A'
mCD8::GFP
B'
mCD8::GFP
A''
NCad
B''
ECad
C
NCad::Cherry
ECad::GFP
C'
NCad::Cherry
C''
ECad::GFP
D
PG
SPG
WG
Ax
E
PG
SPG
WG
Ax
F
Dlg5::GFP NCad:cherry
G
Dlg5::GFP ECad:cherry
F'
NCad::cherry
G'
ECad::cherry
F''
Dlg5::GFP
G''
Dlg5::GFP

# Figure 5

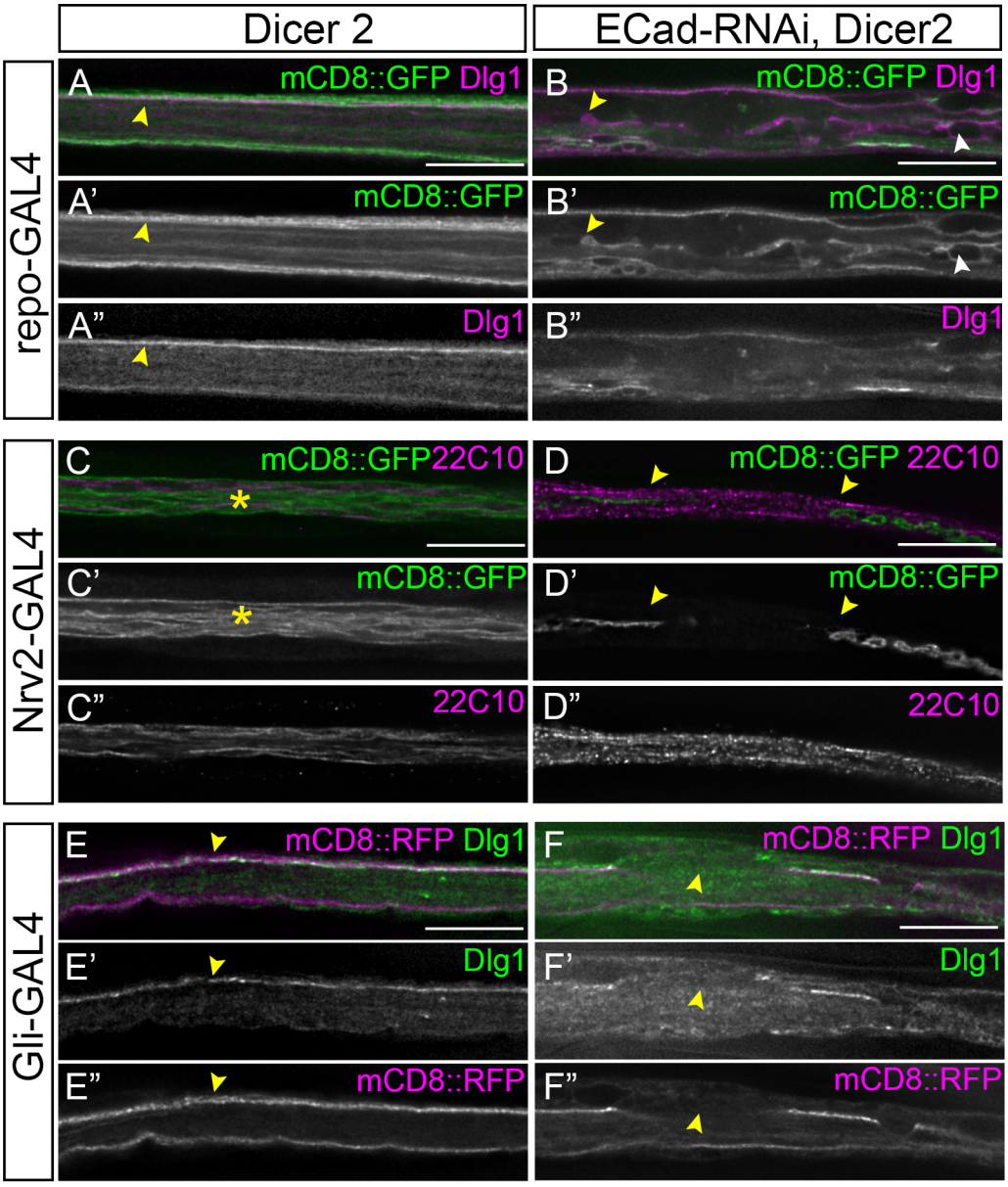
Dicer 2
ECad-RNAi, Dicer2
repo-GAL4
A
mCD8::GFP Dlg1
B
mCD8::GFP Dlg1
A'
mCD8::GFP
B'
mCD8::GFP
A"
Dlg1
B"
Dlg1
Nrv2-GAL4
C
mCD8::GFP22C10
D
mCD8::GFP 22C10
C'
mCD8::GFP
D'
mCD8::GFP
C"
22C10
D"
22C10
Gli-GAL4
E
mCD8::RFP Dlg1
F
mCD8::RFP Dlg1
E'
Dlg1
F'
Dlg1
E"
mCD8::RFP
F"
mCD8::RFP

# Figure 6

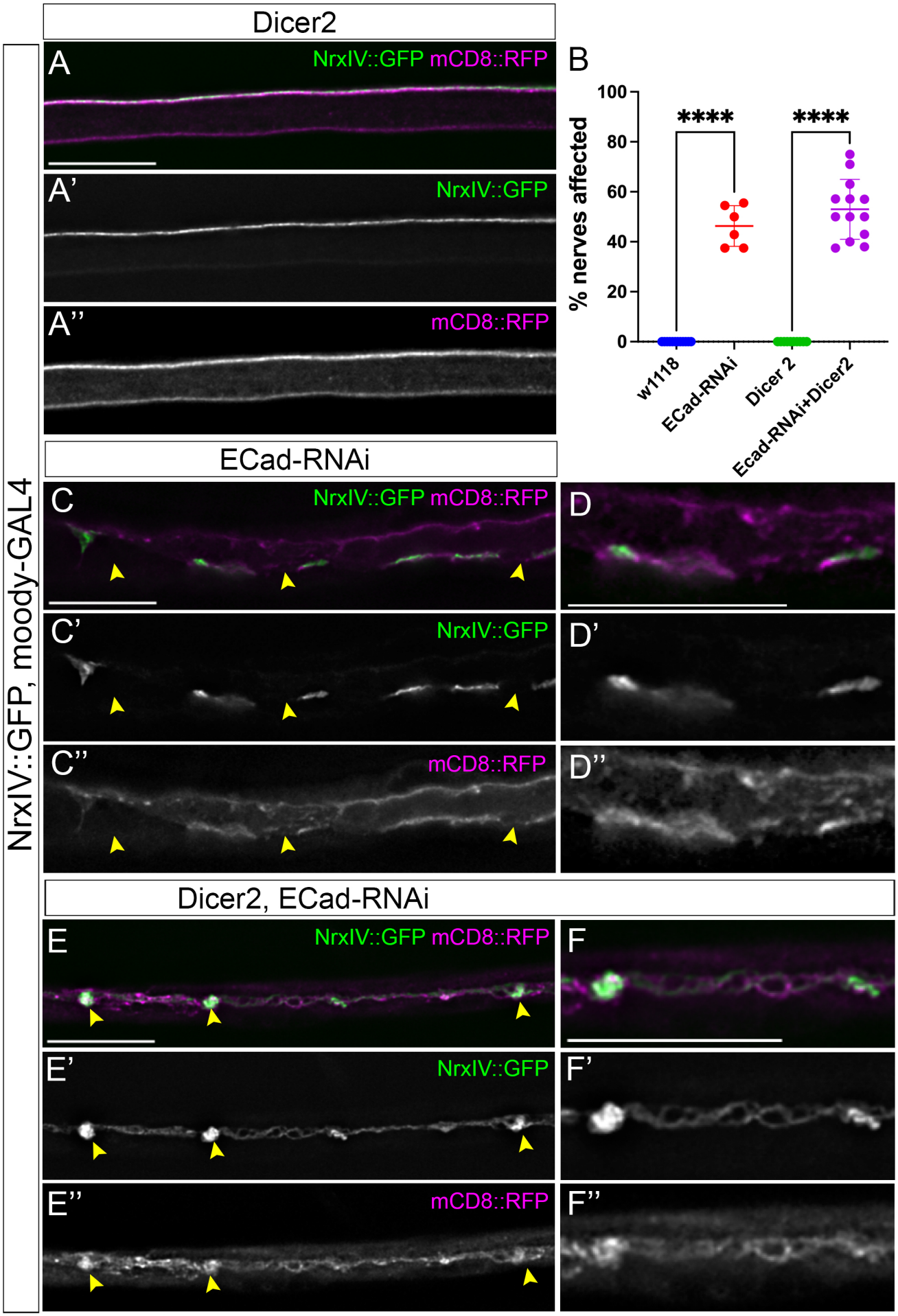
NrxIV::GFP, moody-GAL4
Dicer2
A
NrxIV::GFP mCD8::RFP
A'
NrxIV::GFP
A''
mCD8::RFP
B
% nerves affected
100
80
60
40
20
0
****
****
w1118
ECad-RNAi
Dicer 2
Ecad-RNAi+Dicer2
ECad-RNAi
C
NrxIV::GFP mCD8::RFP
D
C'
NrxIV::GFP
D'
C''
mCD8::RFP
D''
Dicer2, ECad-RNAi
E
NrxIV::GFP mCD8::RFP
F
E'
NrxIV::GFP
F'
E''
mCD8::RFP
F''

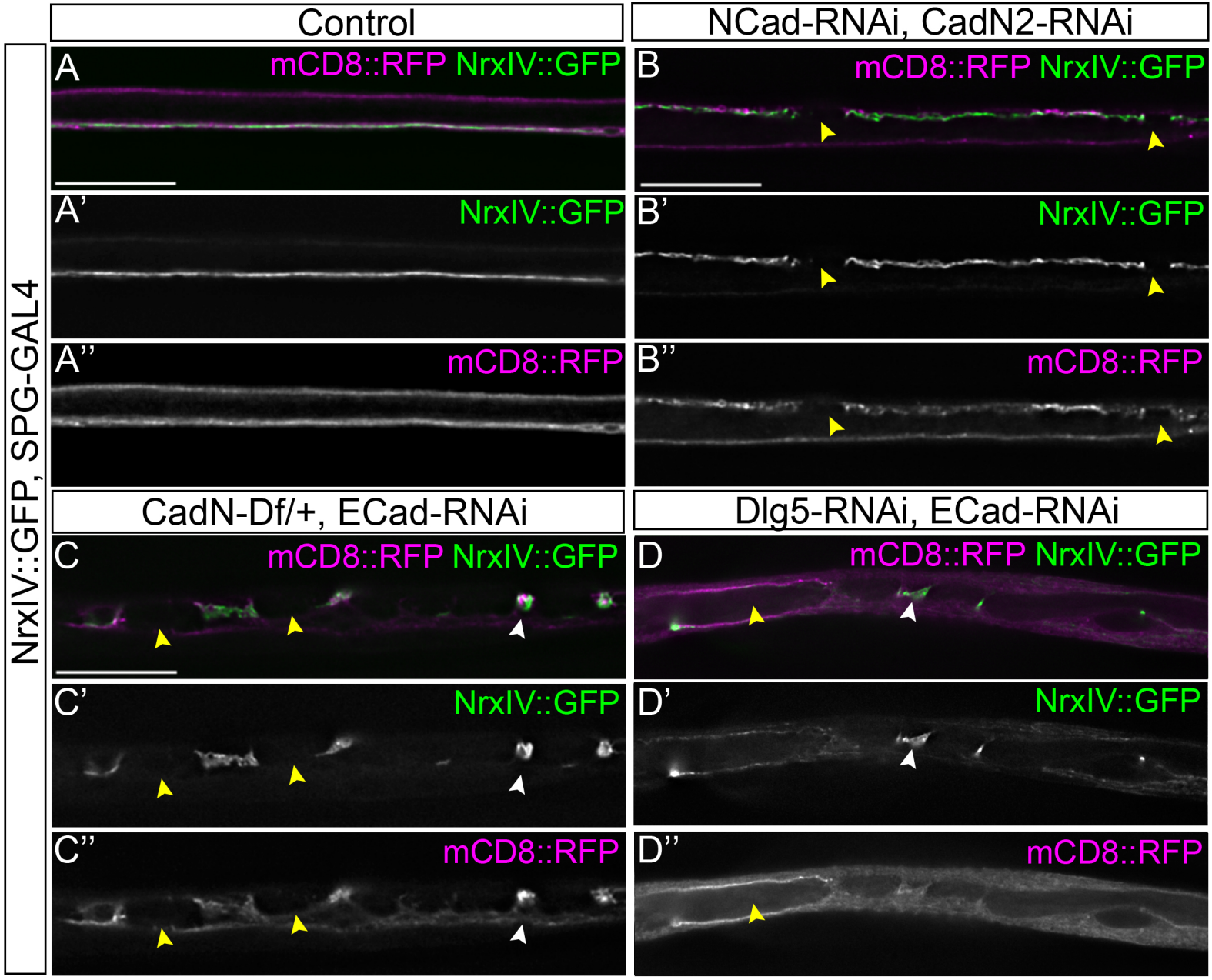
Control
NCad-RNAi, CadN2-RNAi
NrxIV::GFP, SPG-GAL4
A
mCD8::RFP NrxIV::GFP
B
mCD8::RFP NrxIV::GFP
A'
NrxIV::GFP
B'
NrxIV::GFP
A''
mCD8::RFP
B''
mCD8::RFP
CadN-Df/+, ECad-RNAi
Dlg5-RNAi, ECad-RNAi
C
mCD8::RFP NrxIV::GFP
D
mCD8::RFP NrxIV::GFP
C'
NrxIV::GFP
D'
NrxIV::GFP
C''
mCD8::RFP
D''
mCD8::RFP

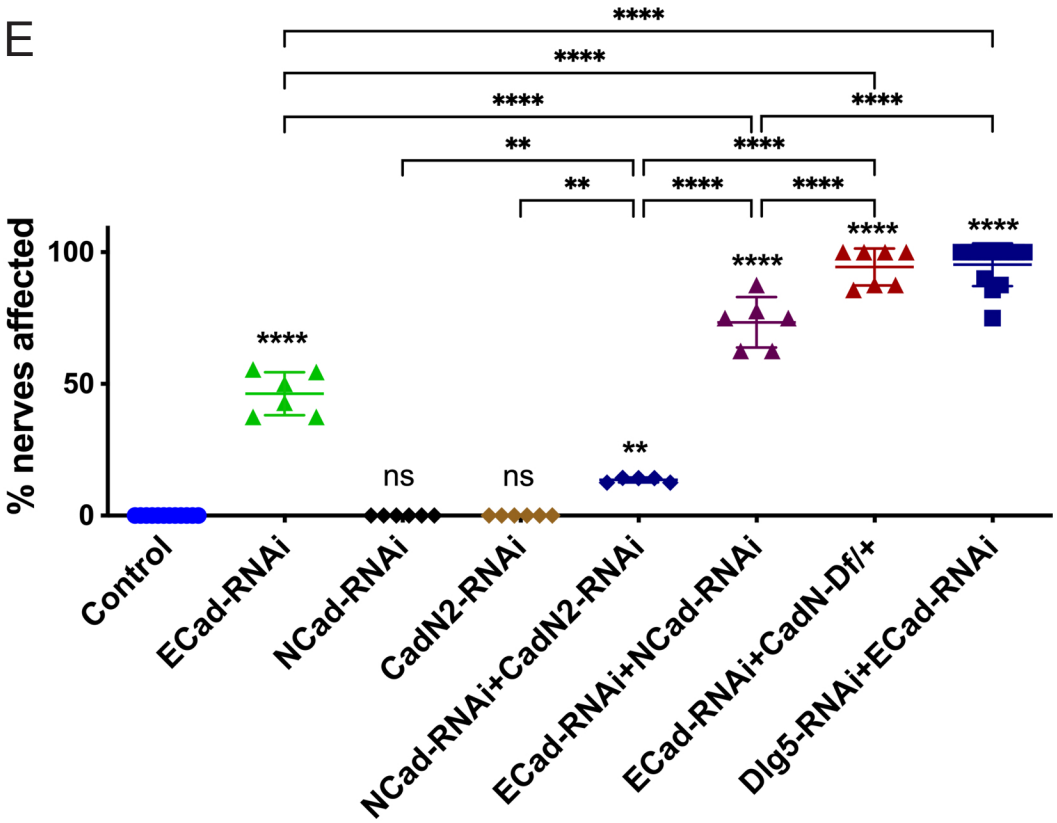
E
% nerves affected
100
50
0
****
ns
ns
**
****
****
****
Control
ECad-RNAi
NCad-RNAi
CadN2-RNAi
NCad-RNAi+CadN2-RNAi
ECad-RNAi+NCad-RNAi
ECad-RNAi+CadN-Df/+
Dlg5-RNAi+ECad-RNAi

Figure 8

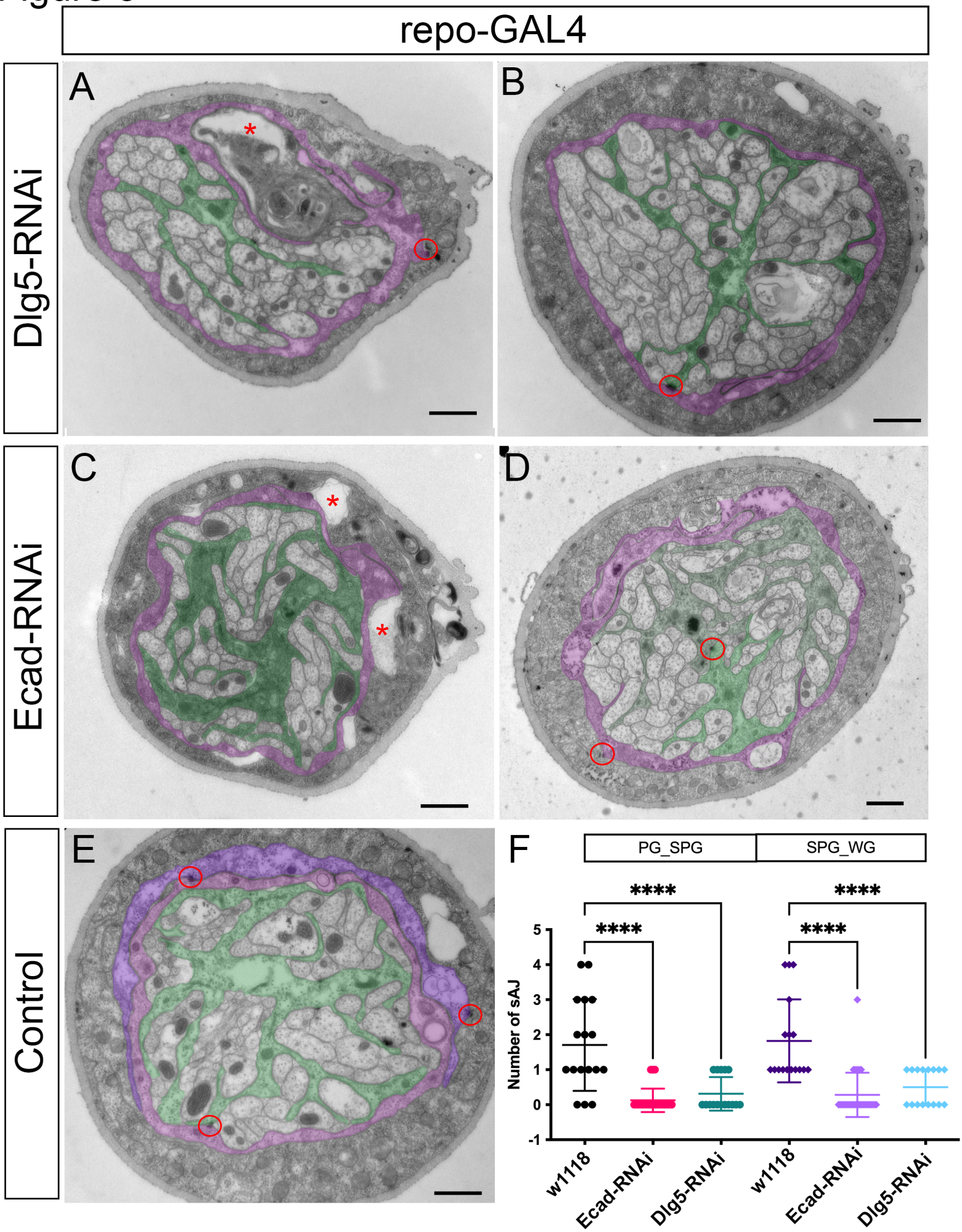
repo-GAL4
Dlg5-RNAi
Ecad-RNAi
Control
A
B
C
D
E
F
PG_SPG
SPG_WG
****
****
****
****
Number of sAJ
5
4
3
2
1
0
-1
w1118
Ecad-RNAi
Dlg5-RNAi
w1118
Ecad-RNAi
Dlg5-RNAi

Figure 9

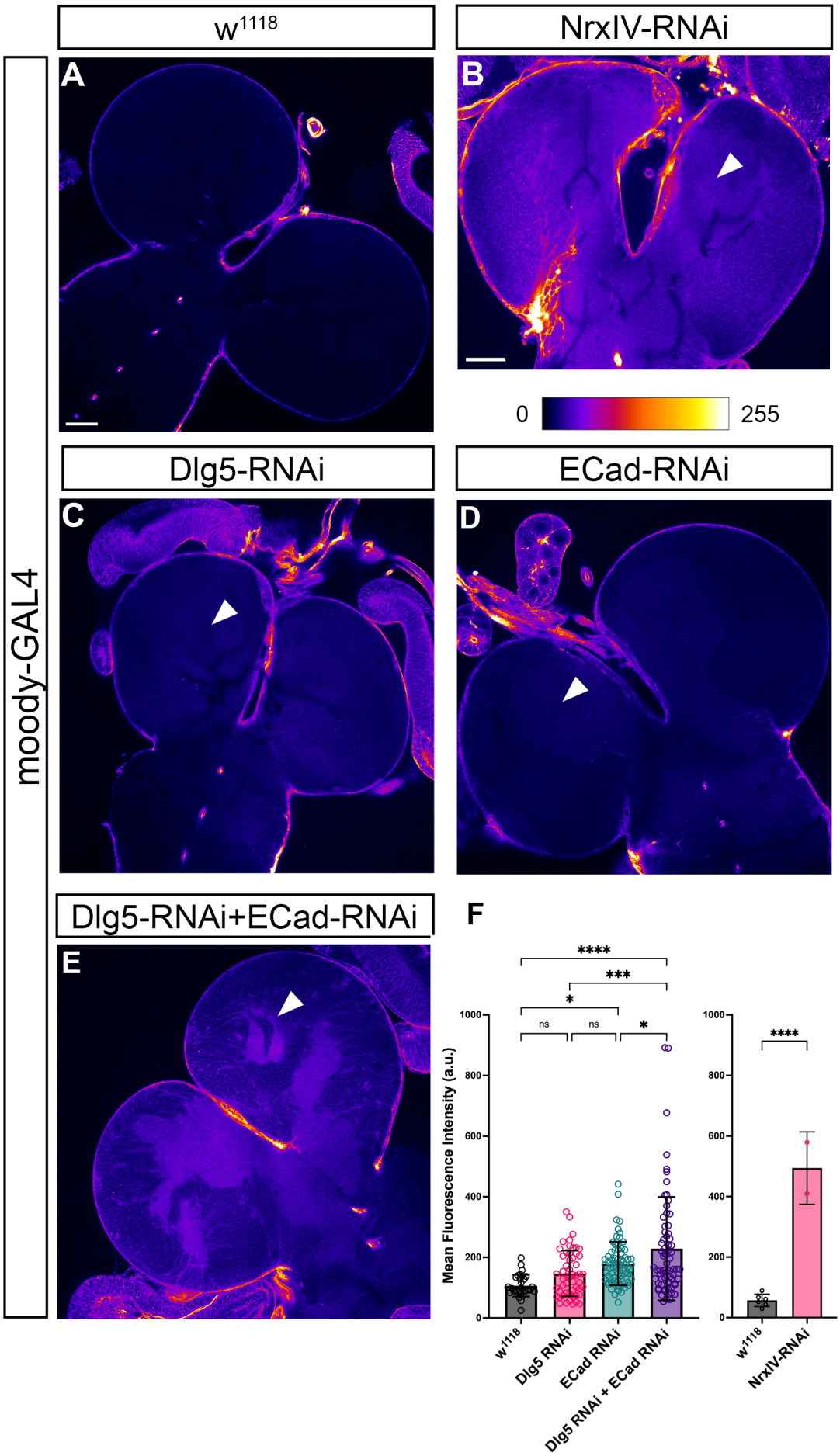
w1118
NrxIV-RNAi
moody-GAL4
A
B
0
255
Dlg5-RNAi
ECad-RNAi
C
D
Dlg5-RNAi+ECad-RNAi
E
F
Mean Fluorescence Intensity (a.u.)
1000
800
600
400
200
0
****
***
*
ns
ns
*
****
w1118
Dlg5 RNAi
ECad RNAi
Dlg5 RNAi + ECad RNAi
w1118
NrxIV-RNAi

Figure 10

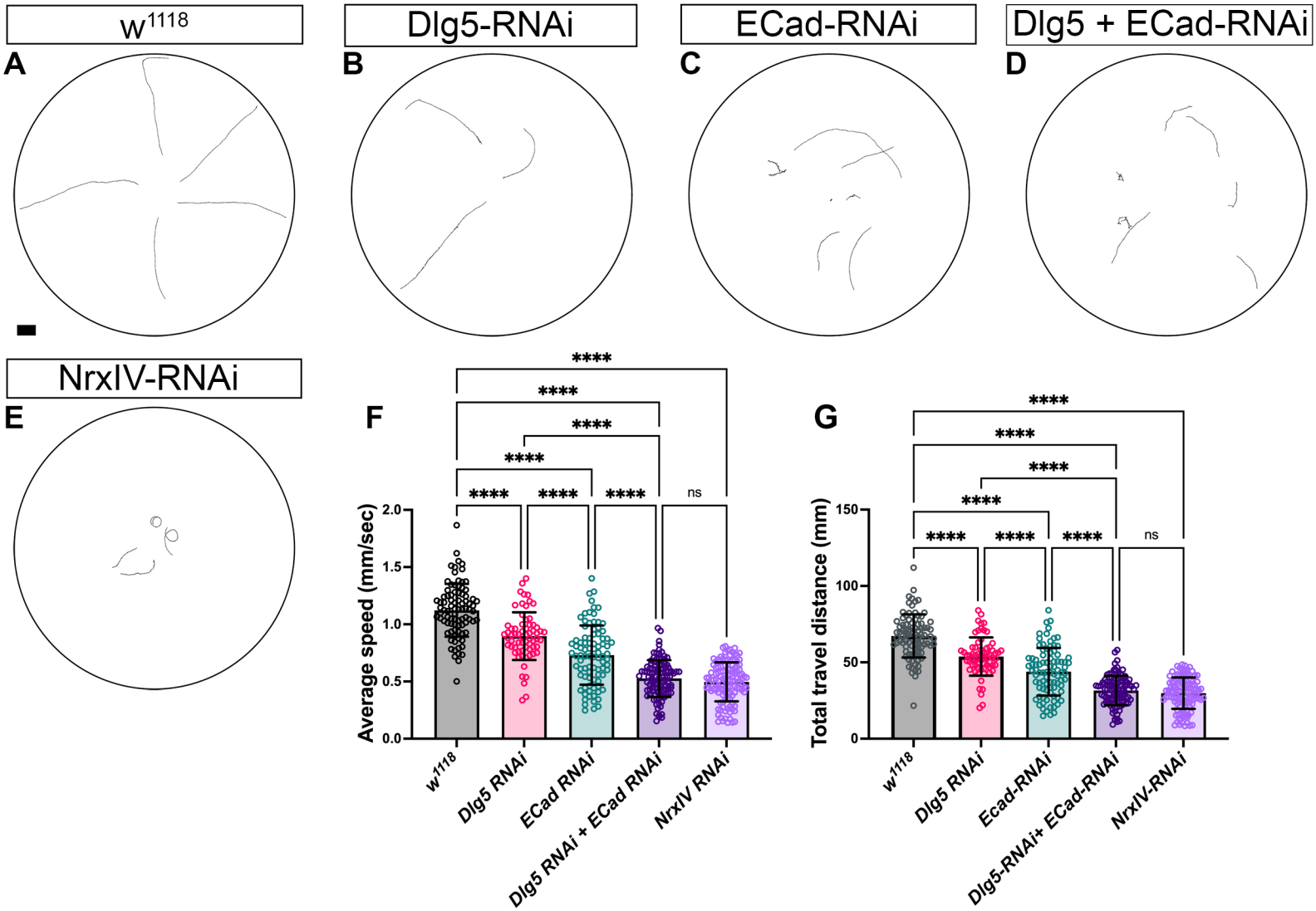
w1118
Dlg5-RNAi
ECad-RNAi
Dlg5 + ECad-RNAi
A
B
C
D
NrxIV-RNAi
E
F
G
Average speed (mm/sec)
2.0
1.5
1.0
0.5
0.0
****
ns
w1118
Dlg5 RNAi
ECad RNAi
Dlg5 RNAi + ECad RNAi
NrxIV RNAi
Total travel distance (mm)
150
100
50
0
Ecad-RNAi
Dlg5-RNAi+ ECad-RNAi
NrxIV-RNAi